

Advancing Precision Agronomy for Minimizing Production Risk

by

Md. Samiul Alam (1179715)
B.Sc. (Computer Science and Engineering),
Ahsanullah University of Science and Technology, Dhaka, Bangladesh

A Thesis Submitted in Partial Fulfillment of the Requirements for the Degree of
Master of Environmental Studies
in the Department of Geography and the Environment

Supervisory Committee: Dr. Muditha Heenkenda
Dr. Kamil Zaniewski
Dr. Tarlok Singh Sahota

Examining Committee: Dr. Muditha Heenkenda
Dr. Kamil Zaniewski
Dr. Tarlok Singh Sahota
Dr. Dilshan Benaragama (External examiner)

The thesis is accepted by the
Dean of Graduate Studies
LAKEHEAD UNIVERSITY
April 2024

Abstract

Farming in Northwestern Ontario faces unique challenges, including a shorter growing season, severe weather conditions, and limited infrastructure and support services. Despite these obstacles, the region holds great potential for expanding agricultural production, particularly for crops like soybeans. Soybean, a crop of significant economic and nutritional value, is susceptible to pests, diseases, and environmental stresses that reduce productivity. Effective health monitoring is crucial to optimize yields and quality. This study explored the use of low-cost proximal field cameras and remote sensing techniques for monitoring soybean leaf chlorophyll. A Mapir Survey3W camera was selected to capture high spatial resolution images in the green, red, and near-infrared regions of the electromagnetic spectrum. The optimal camera setup was investigated by comparing vertical (90°) and oblique (45°) orientation angles and automating image capture using a Raspberry Pi 4 Model B powered by a solar panel system. The vertical camera showed higher spectral reflectance values, while no significant difference was detected for vegetation indices. Once a series of images were captured using the identified optimal camera configurations, the images were preprocessed to obtain spectral reflectance values. Vegetation indices, such as the Green Normalized Difference Vegetation Index (GNDVI), were calculated from the captured images over the growing season. For calibration and validation purposes, at each field visit (within 7-10 days time), soybean leaf chlorophyll content (LCC) was measured using Apogee Instruments MC-100 Chlorophyll Meter. The correlation between GNDVI and LCC was established over time using the inverse function of piecewise linear regressions. The robustness of the regression models was measured by a Kolmogorov–Smirnov statistical comparison test between the predicted LCC over time and the field-measured LCC. The results were statistically not significant, indicating the similarity between the two data sets. Finally, a user-friendly prototype software application was built to make the proposed model accessible to the public. This study provided valuable insights into the optimal setup of field cameras and the use of low-cost remote sensing techniques for soybean leaf chlorophyll monitoring. The proposed methodologies and analyses contribute to the remote sensing techniques in agriculture using affordable sensors, supporting sustainable agriculture practices, and minimizing production risks in soybean cultivation.

Acknowledgment

This work was supported by the Agriculture and Agri-Food Canada [grant number: ARI-IAR-MG 23, June 25th, 2021]; and the Lakehead University Agriculture Research Station Agriculture Research Capacity Development Fund [grant number 1468376, July 22nd, 2021]. I would like to express my sincere gratitude to the thesis committee members for the unparalleled support and guidance I have received. I would like to thank the technicians at the Lakehead University Agriculture Research Station (LUARS) for their diligent care of the experimental soybean plots. I am also deeply appreciative of the contributions made by Jason Freeburn and Reg Nelson at the Department of Geography and the Environment in setting up the camera sensors in the field. I extend my heartfelt thanks to the research team at the Department of Crop and Soil Sciences and the Department of Electrical and Computer Engineering, North Carolina State University, USA, for their invaluable support during the development of the camera system. Finally, I would like to acknowledge the significant contribution of Revanth Yenugudhati in developing the Python scripts to automate the image-capturing procedures. The support, collaboration, and expertise of all those mentioned above have been crucial to the successful completion of this thesis, and I am truly grateful for their involvement.

Table of Contents

Chapter 1: General Introduction	1
1.1 Chapter Synopsis	3
Chapter 2: Optimizing the Image Capturing Workflow to Assess Soybean Health Properties.....	4
2.1 Introduction.....	4
2.2 Materials and Method	7
2.2.1 Study area	7
2.2.2 Camera selection and set up.....	8
2.2.3 Data processing and analysis	11
2.3 Results	15
2.3.1 Ground coverage and pole structure	15
2.3.2 Camera selection and settings.....	15
2.3.3 Image analysis.....	17
2.4 Discussion	21
2.4.1 Optimized camera parameters.....	21
2.4.2 Camera orientation.....	22
2.4.3 Operational cost	23
2.5 Conclusions	23
Chapter 3: Monitoring Soybean Leaf Chlorophyll Content Using Low-Cost Remote Sensor.....	25
3.1 Introduction.....	25
3.2 Data and Method	29
3.2.1 Study area and data collection	29
3.2.2 Data processing and analysis	31
3.2.3 Building the prototype web application.....	33
3.3 Results	33
3.4 Discussion	38
3.4.1 Limitations and further recommendations	39
3.5 Conclusions.....	40

Chapter 4: Conclusions and Recommendations for Future Research.....	43
4.1 Low-cost Remote Sensing System for Soybean Monitoring.....	43
4.2 Limitations and Future Recommendations	44
References.....	46

List of Tables

3.1 vegetation indices formula.....	14
Table 2.2 Spectral resolution of MAPIR Survey 3W RGN Camera	16
Table 2.3 The estimated cost breakdown of the experimental setup	16
Table 2.4 Classification results (percentages) for each reproductive stage	17
Table 3.1 Spectral resolution of MAPIR Survey 3W Camera.....	29

List of Figures

Figure 2.1 A map of the Lakehead University Agriculture Research Station, Thunder Bay, Ontario, Canada. The location of the camera (yellow point) and a soybean plot (red polygon) are shown on the map	8
Figure 2.2 The camera set up: (a) the camera oriented at 90°; (b) the camera oriented at 45°; (c) the power supply (battery and the box); (d) the wooden box for the Raspberry Pi computer, controller and other accessories; and (e) solar panel	11
Figure 2.3 Individual leaf segment using the watershed algorithm. (a) the whole image, bottom right, shows an outline of nine small moving windows; (b) shows the zoomed area over a corner of the blocked image; (c) shows the segmented smaller blocks	13
Figure 2.4 Sample standard false-color images taken from R4 reproductive stage (a) the image from 90° camera and (b) the image from 45° degree camera.	15
Figure 2.5 Change of spectral reflectance values in (a) Red, (b) Green, and (c) NIR bands over time for both 90° and 45° cameras. The dots represent mean spectral reflectance values for each leaf segment at a certain time, and the blue and orange lines are the best-fitted line among the points.....	19
Figure 2.6 NDVI values over time (R4-7 stages): (a) 90° camera and (b) 45° camera. The blue dots represent mean NDVI values for each leaf segment over time, and the blue line is the best-fitted line for those points.	20
Figure 2.7 GNDVI values over time (R4-7 stages): (a) 90° camera and (b) 45° camera. The blue dots represent mean GNDVI values for each leaf segment over time, and the blue line is the best-fitted line for those points.	20

Figure 2.8 SAVI values over time (R4-7 stages): (a) 90° camera and (b) 45° camera. The blue dots represent mean SAVI values for each leaf segment over time, and the blue line is the best-fitted line for those points.21

Figure 3.1 A map of the Lakehead University Agriculture Research Station, Thunder Bay, Ontario, Canada. The location of the camera (yellow points) and a soybean plot (red polygon) are shown on the map30

Figure 3.2 Individual leaf segment using the watershed algorithm. (a) the whole image divided into smaller blocks of windows; (b) shows the zoomed area over a small block; (c) shows the segmented smaller blocks using the watershed algorithm; (d) shows the final constructed individually segmented image after convolution.....31

Figure 3.3 Geen Normalized Difference Vegetation Index (GNDVI) change over time; (a) GNDVI changes with respect to no. of days from seeding; (b) GNDVI values overlayed with the best-fitted piecewise linear regression models.....34

Figure 3.4 Leaf Chlorophyll Concentration ($\mu\text{mol m}^{-2}$) change over time; (a) LCC changes with respect to no. of days from seeding; (b) LCC values overlayed with the best-fitted piecewise linear regression models.....34

Figure 3.5 Predicted Leaf Chlorophyll Concentration ($\mu\text{mol m}^{-2}$) change over time derived using the equation (5)35

Figure 3.6 Top row: Original RGB image captured (with a Samsung Note 20 Phone Camera) on the same date the corresponding RGN images were captured; Middle row: Corresponding RGN image; Bottom row: Corresponding chlorophyll distribution image.....36

Figure 3.7 An example of the web application interface to map leaf chlorophyll content.....37

Chapter 1: General Introduction

Northwestern Ontario (NWO), Canada, has a cold climate with a relatively short growing season compared to the southern parts of the province. The continuously changing and unpredictable weather makes agricultural practices more challenging (Chapagain, 2017). Despite these challenges, NWO holds significant potential for agriculture, with fertile soils, good transportation networks, and affordable land (Chapagain, 2017). However, farming in the region faces numerous challenges, including a short growing season, unpredictable weather, and a lack of support services (Chapagain, 2017). The impact of climate change further exacerbates these challenges, necessitating the adoption of new farming techniques. One such technique is precision agriculture, which is gaining traction in the region (Shafi et al., 2019). Precision agriculture (PA) offers a suite of technologies and methodologies that can significantly mitigate the agricultural challenges faced in Northwestern Ontario (NWO), particularly those related to the short growing season, unpredictable weather, and the broader impacts of climate change. By integrating advanced technologies such as remote sensing, geographic information systems (GIS), and other digital tools, PA enables more precise management of field variations, enhancing both the efficiency and sustainability of agricultural practices (Rimpika et al., 2023; Shafi et al., 2019).

The short growing season in NWO limits the window for crop growth and maturation, necessitating highly efficient farming practices to maximize yield within this constrained timeframe (Sahota et al., 2013). Precision agriculture can address this challenge by optimizing planting schedules and crop selection (Sajid & Hu, 2022). Technologies such as remote sensing allow for detailed analysis of crop health across different parts of a farm, enabling farmers to closely and precisely monitor crop health variations that help them to make better decisions (Omia et al., 2023).

With the advancement of remote sensing technologies, such as satellite imagery, drones, ground sensors, and artificial intelligence (AI), a new era of precision agriculture is booming. These technologies enable farmers to monitor crop health, growth stages, moisture levels, and other key indicators at a much finer spatial and temporal resolution than traditional methods (Omia et al., 2023; Sishodia et al., 2020). By integrating this real-time data with weather forecasts, soil maps,

and crop models, farmers are empowered to make more informed decisions on irrigation, fertilization, pest control, and harvest timing. This optimizes yields and quality and minimizes inputs and environmental impacts, heralding a more sustainable future for agriculture. (Han et al., 2024).

Adopting precision agriculture systems also comes with challenges, especially for small and medium-sized farms (Omia et al., 2023). The high upfront costs of equipment and software, the need for technical skills and training, and the lack of interoperability between different data sources and platforms can be barriers to entry (Omia et al., 2023). Another concern is ensuring data privacy, ownership, and security (Kaur et al., 2022). Further research is necessary to develop more affordable, user-friendly, and scalable precision agriculture solutions that are adapted to the specific needs and constraints of farmers, especially in NWO and nearby regions.

Climate change has enabled farmers to try new varieties of crops in the NWO region. Soybean is such an important crop that is becoming increasingly popular in this region (Pearce, 2024). The short growing season of NWO, fewer risks compared to its alternative crops like Canola, and more profit margins are some of the reasons behind its increasing popularity (Pearce, 2024). In 2022, soybeans were cultivated over a total of 3 million acres of land in Ontario (Pearce, 2024). Soybean has a market size of over 4.4 billion dollars in Ontario in 2024 (Kaur et al., 2022). Though the main use of Soybean is to produce Soybean oil, it is also considered one of the richest protein sources for people and animal diets (Pagano & Miransari, 2016). Soybean oil is used as a key ingredient in many industries like paint, adhesives, fire extinguishers, etc. (Johnson & Myers, 1995). Considering its importance, a continuous monitoring system for Soybeans needs to be built.

The main aim of this project was to explore the potential of a remote sensing-based precision agriculture system that utilizes low-cost remote sensors to deliver robust, easy-to-understand information to farmers, enabling the precision application of fertilizers and other inputs for soybean crops. To achieve this goal, the identified three specific research objectives were to: a) determine the optimal properties and orientation of proximal remote sensors for capturing high-quality images of soybean canopies; b) correlate remotely sensed data and field observations to predict the spatial distribution of leaf chlorophyll content of test plots; and c) design and develop a prototype, user-friendly software application to deliver useful information to farmers.

1.1 Chapter Synopsis

Chapter 1: General Introduction

This chapter provides the theoretical background and historical studies that have led to the research reported in the dissertation, followed by the research's significance. A significant gap in the current state of knowledge regarding the use of low-cost remote sensors in precision farming is demonstrated. The research aim, and three specific objectives were identified in this chapter.

Chapter 2: Optimizing the image capturing workflow to assess Soybean health properties

This chapter explored the optimal setup and parameters for using proximal field cameras to monitor soybean health (specific objective (a)). The study aimed to determine the optimal camera type, setup parameters (orientation angles, camera settings, cost-friendly setup), power supply, data storage, and automation of image capture. The work was reported in a format suitable for submission as a rapid communication to “Remote Sensing Letters.”

Chapter 3: Monitoring Soybean Leaf Chlorophyll Using Low-Cost Remote Sensor

This chapter introduced new data relating to the specific objectives (b) and (c). The work was reported as a journal article as it will be submitted to the “International Journal of Remote Sensing” in the future. A robust relationship between soybean leaf chlorophyll content and vegetation index has been established, which is later used for the development of the prototype web application.

Chapter 4: Conclusions and Recommendations for Future Research.

The concluding chapter explicitly detailed the contribution of this thesis to the field of precision agriculture and remote sensing. It revisits the main findings and techniques used throughout each preceding chapter, describing how the approach and results are significant, new, and innovative. Finally, there are some suggestions for study objectives and improvements in future research.

Chapter 2: Optimizing the Image Capturing Workflow to Assess Soybean Health Properties

2.1 Introduction

Soybean is a widely cultivated crop used for various purposes, including animal feed, biodiesel production, and human consumption (Stein et al., 2008). As a source of protein and other essential nutrients, soybeans are an important part of the global food supply (Funk, 2020). However, soybean plants are vulnerable to various pests, diseases, and environmental stresses, which can significantly reduce their productivity and quality (Haskett et al., 2000; Lal et al., 1999).

Farmers and researchers use various methods to monitor Soybean health, such as visual inspection of plants, laboratory analysis of nutrient levels of plants and soil properties, and remote sensing (Omia et al., 2023). Most remote sensing methods include analyzing satellite images and aerial photographs for crop monitoring (Sishodia et al., 2020). Satellite imagery fails to provide high spatial resolution images for a low or reasonable cost. Temporal resolution is also a drawback to satellite imagery. Satellites have their pre-defined orbit and, thus, a fixed revisit time. Low temporal resolution can be a problem in regions where the weather changes rapidly, as it can lead to inaccurate or delayed crop monitoring and management. Climate studies have shown that certain regions, such as Northwestern Ontario, experience more rapid weather changes than others (Ahmed et al., 2014, 2022). Another drawback to the satellite imagery is that it is not very useful for small-sized farmlands where spatial resolutions are larger than the field size (Sozzi et al., 2018). Generally, satellite imagery accessible to the general public lacks adequate spatial or temporal resolution to monitor and manage crops throughout their growth cycle.

Aerial photography is one of the best methods to monitor vegetation health as the technology provides high spatial and temporal data on demand (Morgan et al., 2010). However, their operational cost is high and requires adequate aircraft, sensors, and skills to acquire, process, and extract information from images (Fensham & Fairfax, 2002). Recently, attention was given to images acquired from Remotely Piloted Aircraft Systems (RPAS). RPASs are an efficient solution to crop health monitoring because of their low operational cost, precision and flexibility, and

accessibility to remote areas (Gayathri Devi et al., 2020). Still, there are a few disadvantages to using RPAS images. Operating RPAS in an agricultural setting may require compliance with regulations like licensing and airspace restrictions. Moreover, safety concerns regarding collisions, privacy, and data security must also be addressed (Hafeez et al., 2023). Adverse weather conditions such as strong winds, rain, or fog can hinder RPAS operations and data collection, limiting their effectiveness. Their power source limits RPAS performance. Even with the latest drone technologies, it is tough to get an hour of power backup from a drone battery (Hafeez et al., 2023). Although these methods provide accurate results promptly, even in real-time, there are operational problems, such as the cost of equipment required and the high level of technical knowledge for image acquisition and processing (Sishodia et al., 2020). A low-cost, reliable option is still in demand for crop health monitoring. The ideal solution would be a proximal sensing camera (hand-held or fixed to a frame) for continuous image acquisition throughout the growing season, an automated image processing algorithm, and an application to disseminate results.

Fixed field cameras are stationary cameras installed in specific locations to capture images or data over an extended period. Depending on the particular application, they can be equipped with various sensors—optical, infrared, or multispectral cameras (Bogue, 2017). They provide continuous monitoring capabilities and help long-term trend and pattern analysis in the observed area. These cameras offer several advantages over other remote sensing methods, such as higher spatial and temporal resolutions and lower operational costs (Mahajan et al., 2017; Nijland et al., 2014; Peng et al., 2019; Phadikar & Goswami, 2016; Ramos-Giraldo, Reberg-Horton, Locke, et al., 2020; Ramos-Giraldo, Reberg-Horton, Mirsky, et al., 2020; Singh & Misra, 2017). Field cameras and other sensors are becoming increasingly popular for monitoring crop health, weather parameters, and soil conditions, especially for small-sized farms, as they provide a cost-effective method for collecting data over a particular area. These sensors have been mounted on farm machinery, purpose-built robots, and at fixed locations (Bogue, 2017). A limited number of studies have used fixed cameras for crop health monitoring so far; Li et al., 2021 aimed to find the best camera viewing angle and setup for capturing the 3D point clouds. The study confirmed that the oblique imagery provided the best estimation for leaf length and width, and the oblique and nadir angles were the best for modeling canopy and leaf parameters (Li et al., 2021). The study suggested that oblique imagery is a promising approach for crop monitoring using a single-camera platform.

One of the key properties of proximal sensing cameras that affects their performance in crop monitoring is spatial resolution. Higher spatial resolution cameras can capture more detailed crop canopy images, improving growth monitoring accuracy (J. Zhang et al., 2020). The ability to capture large amounts of data quickly and efficiently is vital to plant phenology monitoring and has the ability to detect subtle changes in plant health that might not be visible to the naked eye (Kross et al., 2011). Fujiwara et al., 2022 confirmed that the camera angle from an RPAS can affect the accuracy of estimating maize plant height. However, how camera angle can affect the captured image data from a proximal field camera is still not explored. A research team from North Carolina State University used a fixed camera to monitor the drought status of soybean plants in a field experiment (Ramos-Giraldo, Reberg-Horton, Locke, et al., 2020). They could predict crop plants' drought status with more than 80% accuracy relative to expert-derived visual drought ratings. In another experiment, they achieved an accuracy of 74% with the embedded machine-learning algorithm when classifying water stress in soybeans (Ramos-Giraldo, Reberg-Horton, Mirsky, et al., 2020).

To date, no study has explored the comprehensive optimal parameters (camera orientation, pole height, power supply, etc.) for setting up fixed cameras for Soybean health monitoring. Fixed cameras have great potential for assessing soybean health, but their image-capturing workflow for this purpose requires further investigation. This study aimed to explore the optimal fixed camera setup for capturing high-quality images of soybean plants. The specific objectives were to: (1) decide on the suitable low-cost camera that can be used to capture plant variations; (2) set up cameras in the field (pole height, attachments, camera parameters); (3) identify the most suitable camera orientation angle and sun orientation direction; (4) decide on the power supply and data storage; and (5) automate the image capturing process. The second phase of this project would be to automate the image analysis process and develop a mobile application that provides Soybean health parameters on demand.

2.2 Materials and Method

2.2.1 Study area

The study was conducted at the Lakehead University Agricultural Research Station (LUARS) located in Thunder Bay, Ontario, Canada (48.3052° N, 89.3882° W) (Figure 2.1). The research station serves as a principal facility for the establishment, execution, advancement, and dissemination of agricultural research to foster expansion and crop diversification within the agricultural sector. This is achieved through the utilization of small-plot research and extension activities, community-centered agricultural research, and resource management endeavors (Lakehead University Agricultural Research Station).

Thunder Bay is located in Northwestern Ontario (Figure 2.1) and has a humid continental climate. The area experiences four distinct seasons, with warm summers and cold winters. Thunder Bay has an average annual temperature of 3.2°C, with the warmest month being July, with an average temperature of 17.4°C, and the coldest month being January, with an average temperature of -13.6°C (Ahmed et al., 2014). The area receives an average of 840 mm of precipitation annually, with the majority of the precipitation occurring in the summer months. Hence, rainfed agriculture is dominant in the region.

The experimental soybean plots were located in the northeastern section of the LUARS (Figure 2.1). The Soybean was seeded on June 14, 2022, in a grid block pattern, with each block sizing about 1 m x 1.2 m and a 0.33 m buffer zone between each plot on a total area of 87 m x 35 m. The crop was harvested on the first week of October 2022.

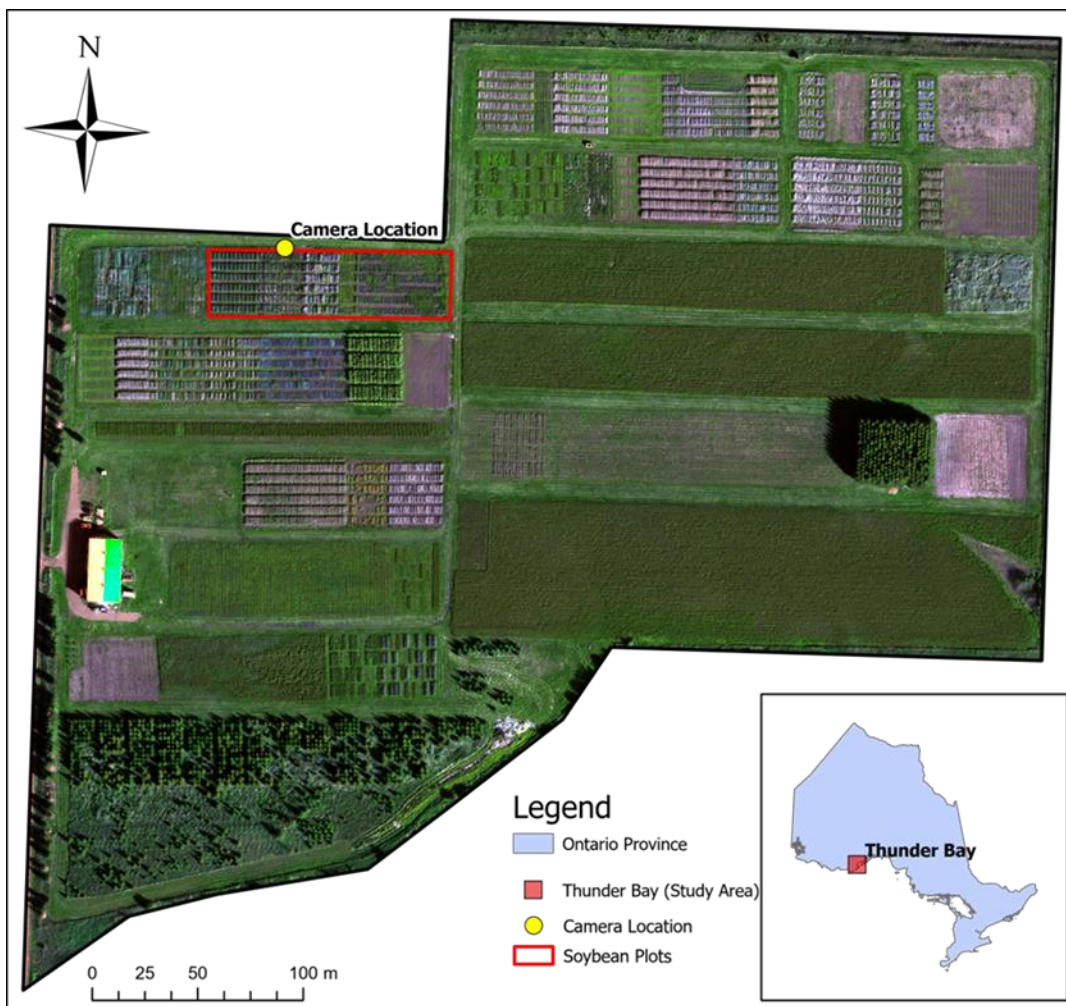


Figure 2.1: A map of the Lakehead University Agriculture Research Station, Thunder Bay, Ontario, Canada. The location of the camera (yellow point) and a soybean plot (red polygon) are shown on the map.

2.2.2 Camera selection and set up.

To optimize the establishment of field cameras, we considered several main requirements (1) good coverage of the plot; (2) selection of suitable camera and camera settings for image acquisition; (3) camera orientation; (4) automated image acquisition and data handling; and (5) continuous power supply for the system.

i) Ground coverage of the plot

The plot's ground coverage varies with the pole's height and the camera's orientation angle (Natural Resources Canada, 2015). When determining the pole height, the following three factors were considered: (a) a footprint of the image should cover at least one soybean plot; (b) Ground Sampling Distance (GSD) of images or in other words, the pixel size should be large enough to identify details up to leaf level; and (c) the camera system should not act as an obstacle to access the plot for agricultural purposes.

ii) Camera selection and camera settings

Camera type: When selecting a camera, the preferences were given to cameras sensitive to the Near Infrared (NIR) region of the electromagnetic spectrum because plants show unique characteristics under exposure to NIR radiation (Lillesand et al., 2015, pp. 14–16). The reflectance of the NIR band on the surface of the leaves can be used to estimate the health status of the crops by calculating vegetation indices (Ustin & Jacquemoud, 2020, Chapter 7).

Camera settings: Camera resolution, shutter speed, aperture, and ISO settings are some important factors that control how much light energy the camera can capture while taking a picture (Jacobson et al. 2013). These parameters were adjusted for capturing images.

iii) Camera Orientation

Pole orientation: The solar elevation, azimuth angle, and viewing angle can play an important role in capturing optimal images (Lillesand et al., 2015, p. 25). Depending on the location and orientation of the pole, plants can be sunlit or shaded. In the northern hemisphere, during the summer, the sun rises northeast and sets northwest. We strategically positioned our pole on the soybean field's north edge (Figure 2.2). The cameras were oriented towards the south to avoid casting shadows during mid-day and receive the maximum amount of sunlight during the day. The entire structure was designed to avoid casting shadows that could interfere with the resulting images.

Polyvinyl Chloride (PVC) pipes were used to build the pole structure. PVC is a very cheap and lightweight but very strong material that can stand in the windy environment of Northwestern

Ontario. To weatherproof the camera, we used some single-use plastic plates as shades to protect the cameras from the rain and overheating from the sun (Figure 2.2).

Camera orientation angles: Camera viewing angle/orientation can play a role in soybean health assessment, as it affects the visibility of different layers of leaves. From a vertical viewpoint (90°), the camera would primarily capture the top layer of leaves, while lower-level leaves become visible from a diagonal/oblique angle. We selected two camera orientation angles: (a) Vertical Camera, (90°); and (b) Oblique Camera (45°) to capture different perspectives and gather comprehensive information about the soybean plants' health (Figure 2.2).

iv) Image acquisition and data handling

The image-capturing system was designed to be fully automated and controlled by a dedicated controller system to minimize human intervention. The cameras were effectively controlled by a Raspberry Pi 4 Model B computer and Python script. The system was programmed to send the Pulse Width Modulation (PWM) signal to the cameras, triggering the shutter and capturing an image every 30 minutes. This automated process was scheduled to run continuously from 7 AM to 5 PM daily. The camera's specific calibration target images were acquired manually to represent different lighting conditions throughout the season. These images were later used to convert DN values into surface reflectance values.

A storage device without data compression or a lossless compression technique is vital to ensure optimal storage of the result images. Sufficient storage capacity should be available to store all the photos without running out of memory. In our study, the images were stored in a 128 GB micro-SD memory card attached to each camera, enabling the capture of images throughout all stages of soybean growth. Subsequently, the images were transferred to external solid-state drive storage for further analysis. This approach ensured the preservation of image quality and allowed for efficient storage and access during the analysis phase.

v) Power supply

To ensure a continuous power supply throughout the Soybean growing season, a 60W Solar Panel was utilized to charge an 80Ah 12V sealed lead-acid battery. This battery served as the power source for the cameras and the Raspberry Pi computer.



Figure 2.2: The camera setup: (a) the camera oriented at 90°; (b) the camera oriented at 45°; (c) the power supply (battery and the box); (d) the wooden box for the Raspberry Pi computer, controller and other accessories; and (e) solar panel.

2.2.3 Data processing and analysis

i) Data pre-processing

The Soybean has two main growth stages: (1) vegetative; and (2) reproductive. There is a total of eight (8) reproductive stages denoted by R1 through R8 (Purcell et al., 2014). This study was conducted from R4 to R7 reproductive stages.

The images were downloaded manually and sorted out based on the time of the day, lighting conditions, and shadows. Some images were discarded. For instance, images that were too dark to

distinguish the subjects or had any unwanted intrusion in a photograph were discarded. Then, the images were separated into different Soybean growing seasons.

Initially, this camera stores images as Digital Numbers (DNs); however, for the remote sensing analysis, they were converted to spectral reflectance values using the calibration panel images and MAPIR Camera Control (MCC) software (Mapir Camera, 2024). The images were then cropped to remove other features (background) and to obtain Soybean only.

ii) Image processing and analysis

The purpose of the image processing was to evaluate the orientation angle of the camera. Hence, the analysis was done in two different ways: (1) classify images based on NIR reflectance values and compare the percentages of different features that appear on the images with two orientation angles; and (2) evaluate the spectral reflectance values for both orientation angles.

a) Image classification

Spectral reflectance can be different based on the viewing angle and the sun's position (Ustin & Jacquemoud, 2020). Both sets of images (each reproductive stage separately) were classified into five classes: (1) Under Exposed Leaves; (2) Properly Exposed Leaves; (3) Over Exposed Leaves; (4) Dark Shadow; and (5) Soil. We randomly selected training pixels for the moderately exposed leaves class using a NIR reflectance threshold from 0.4 to 0.8 for the range of reproductive stages (R4-7). If the value was higher than that, they were labeled as over-exposed; if lower, they were labeled as under-exposed. This is based on the spectral profile of Soybean leaves and some existing studies; for instance, Durante et al., 2014 and (Vásquez et al., 2023) found that the NIR reflectance for healthy Soybeans was approximately 0.6-0.7. After that, a maximum likelihood classifier algorithm (Lillesand et al., 2015, p. 544) was used to classify each image into five classes using ENVI 5.6.2 software (Geospatial Image Analysis Software | ENVI).

b) Spectral Reflectance Analysis

In order to perform a spectral reflectance analysis, information from each leaf needs to be considered. To extract leaf-level reflectance values, individual leaf segmentation is necessary. The watershed algorithm (Kornilov & Safonov, 2018) was used to perform the individual leaf

segmentation. The watershed algorithm treats the image as a topographic map, where brightness represents the height of each point. The algorithm then finds lines that run along the tops of ridges and then floods the image from these ridges to generate a partition into distinct regions (Roerdink & Meijster, 2000). The flood fills basins around local minima in the image, with each distinct basin representing a different object (Kornilov & Safonov, 2018). When the target image contains too many objects that are touching or overlapping each other in complex ways, the watershed algorithm may fail to separate the individual objects properly. This can lead to under-segmentation, where multiple objects are incorrectly merged together (Liu et al., 2023). To address this issue, each image was divided into a moving window of 100 x 100 pixels to segment individual leaves with 3-4 leaves in each. Then, the watershed algorithm was applied to each windowed region and segmented up to leaf level. The same process is applied to all the smaller blocks in the image for segmentation. Segmented blocks were merged back to form the original image. Figures 2.3 (a) and (b) show an example of the selected nine moving windows, and Figure 2.3 (c) shows that portion after segmenting and merging. The process was automated using a Python programming language (Python 3.12.3 Documentation).

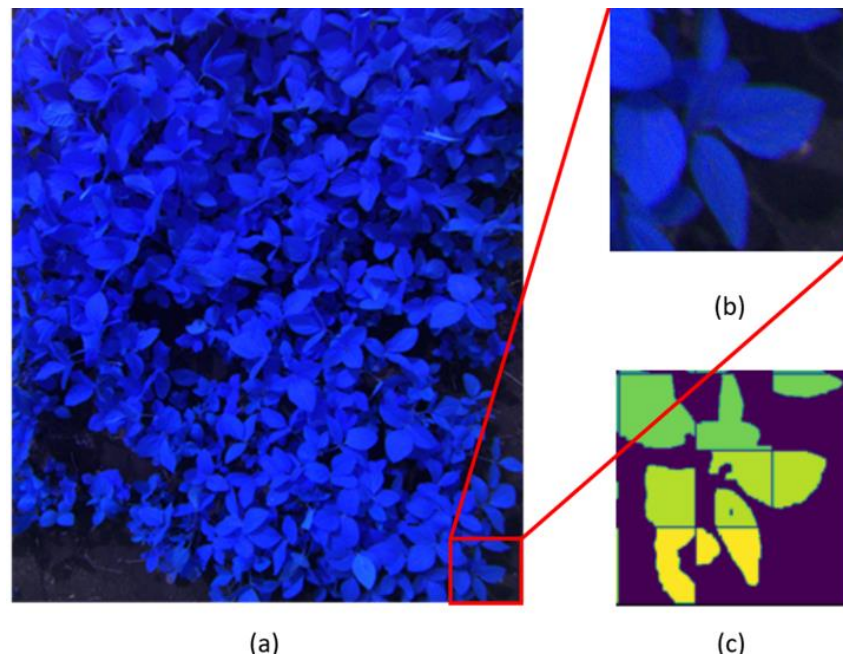


Figure 2.3: Individual leaf segmenting process using the watershed algorithm. (a) the whole image, bottom right, shows an outline of nine small moving windows; (b) shows the zoomed area over a corner of the blocked image; (c) shows the segmented smaller blocks.

After segmenting the image, the spectral reflectance values of individual pixels were extracted, and Vegetation Indices (VIs) were derived (Table 2.1) using the rasterio library of Python programming language (Mapbox, 2018). The mean VI value for each leaf segment was calculated and analyzed against the time. The study used the Normalized Difference Vegetation Index (NDVI), Green Normalized Difference Vegetation Index (GNDVI), and Soil Adjusted Difference Vegetation Index (SAVI) (Table 2.1). We chose these vegetation indices because the camera we used provides us with images in three spectral bands, Red (R), Green (G), and Near Infrared (NIR), and these three vegetation indices can be calculated from the R, G, and NIR values.

Table 2.1: Calculated vegetation indices formula

Vegetation Index	References	Remarks
$NDVI = \frac{NIR - R}{NIR + R}$	(Tucker, 1979)	The NDVI compares the amount of near-infrared light reflected by vegetation to the amount of visible red light reflected by vegetation
$GNDVI = \frac{NIR - G}{NIR + G}$	(da Silva et al., 2020)	The Green Normalized Difference Vegetation Index (GNDVI) is a modified version of the NDVI that uses the green and near-infrared spectral bands better to indicate the variation of chlorophyll content in vegetation. GNDVI has a higher saturation point than NDVI, which means it can be used in crops with dense canopies or in more advanced stages of development (Auravant).
$SAVI = (1 + L) \frac{NIR - R}{NIR + R + L}$	(Huete, 1988)	SAVI minimizes soil influences on canopy spectra by incorporating a soil adjustment factor L into the index. The value of L = 0.5 for Soybeans was adapted from the study: (da Silva et al., 2020).

2.3 Results

2.3.1 Ground coverage and pole structure

The PVC pole structure provides stability in windy environments, positioned at a height of 152 cm, to provide good ground coverage without capturing unnecessary objects (Figure 2.4). The footprint of the images obtained from the vertical camera was approximately 1.5 m x 1m, which just covers one plot and the isle buffer between the adjacent plots (Figure 2.4(a)), and the oblique camera was able to see beyond one plot (Figure 2.4(b)). The ground sampling distance of the images from the vertical camera was approximately 0.07 cm/pixel. Visually, the oblique image (Figure 2.4 (a)) shows both lower and upper-level leaves, but on the contrary, the vertical image (Figure 2.4 (b)) shows mostly the upper-level leaves of soybean plants.



Figure 2.4: Sample standard false-color images taken from R4 reproductive stage (a) the image from 90° camera and (b) the image from 45° degree camera.

2.3.2 Camera selection and settings

The Mapir Survey 3W RGN camera was selected for this study. It is sensitive to the electromagnetic spectrum's green, red, and near-infrared regions (RGN camera) (MAPIR CAMERA, 2023). Table 2.2 shows the central wavelength of each band. The bandwidth of a single band is 15nm.

Table 2.2: Spectral resolution of MAPIR Survey 3W RGN Camera

Spectral Band	Central Wavelength (nm)
Red	660
Green	550
Near Infrared	850

The cameras were equipped with a wide-angle lens to capture a larger field of view. In this study, the bit depth was set to 16-bit, although there are two other options (8-bit and 12-bit) because 16-bit depth can capture more variations of reflectance values than the other two options. The aperture was set to f/2.8, the exposure time was 1/125 sec, and the ISO-100 speed was set to 100. All the images were captured without using a flash or any kind of external light source. The images are saved into two formats: RAW and JPEG, because the MAPIR Camera Control software requires the RAW and JPEG photos to calculate the calibrated reflectance image (Survey3: Multispectral Survey Cameras, 2021).

The construction of the complete experimental camera setup incurred an approximate expenditure of two thousand Canadian Dollars. Detailed estimations of the cost for each component are demonstrated in Table 2.3. It is important to note that these figures exclude any applicable taxes or shipping fees. The procurement of the equipment was primarily facilitated through Amazon Canada, supplemented by purchases from several local stores in Thunder Bay.

Table 2.3: The estimated cost breakdown of the experimental setup

Components	Qty	Estimated Unit Price (CAD)	Estimated Total Price (CAD)
Mapir Survey 3W RGN Camera	2	\$400.00 USD each (Approx. \$514.00 CAD based on the current exchange rate 1 USD = 1.285 CAD on 29 April 2024)	\$1028
Raspberry Pi 4 Model B	1	\$100	\$100
60W Solar Panel	1	\$150	\$150

80 Ah Lead Acid Battery	1	\$180	\$180
PVC pipe for structure	3 m approximately	\$7 per meter	\$21
Cables (Approx. 15 meters)	7 m approximately	\$4 per meter	\$28
Miscellaneous Cost			\$200
Total Cost			\$1707

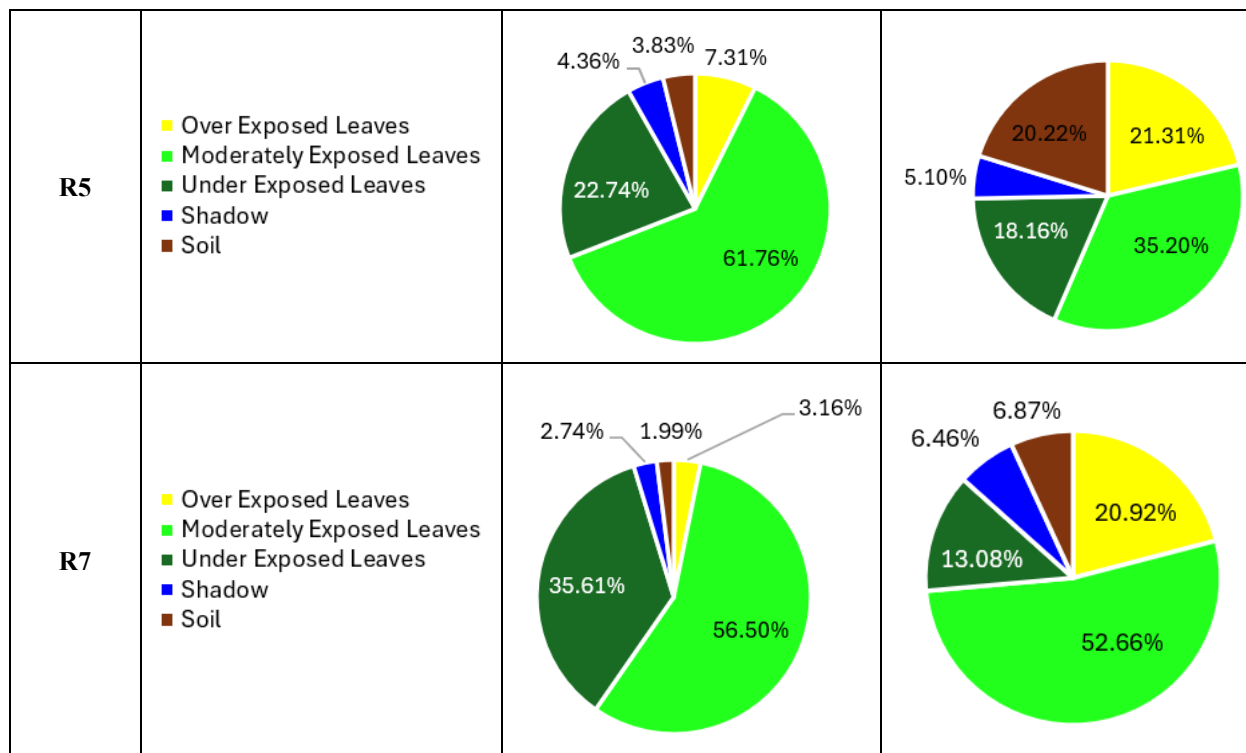
2.3.3 Image analysis

i) Pixel based classification

Table 2.4 shows the pixel-based classification of five different classes at each reproductive stage. When using the vertical camera at the R4 stage, approximately 20% of pixels were overexposed. On the other hand, the oblique camera captured only 3.47% of the pixels in the images that are overexposed. The pattern remains the same throughout the seasons R4, R5 and R7.

Table 2.4: Classification results (percentages) for each reproductive stage

Growth Stages	Classes	Oblique Camera (45°) Pixel Coverage %	Vertical Camera (90°) Pixel Coverage %
R4	<ul style="list-style-type: none"> ■ Over Exposed Leaves ■ Moderately Exposed Leaves ■ Under Exposed Leaves ■ Shadow ■ Soil 		



ii) Spectral reflectance analysis

Figure 2.5 shows how the reflectance value changes over the reproductive stages. Figure 2.3 (a)-(c) indicates that the vertical camera's spectral reflectance values were consistently higher. In Figure 2.5 (a) the differences between the two cameras' red reflectance values are the highest in late August but become similar when they mature. Green (Figure 2.5 (b)) and NIR (Figure 2.5(c)) show a minor difference at the beginning of August (R4) but start to show a very big difference in the later stages. The best-fitted line for green spectral reflectance shows that the oblique camera captures a lot of variations, while the best-fitted line from the vertical camera is more flattened and shows less change over the same time. NIR values of both cameras show approximately similar curves—increasing values from R4, peaking at R5-6, and decreasing (Figure 2.5(c)).

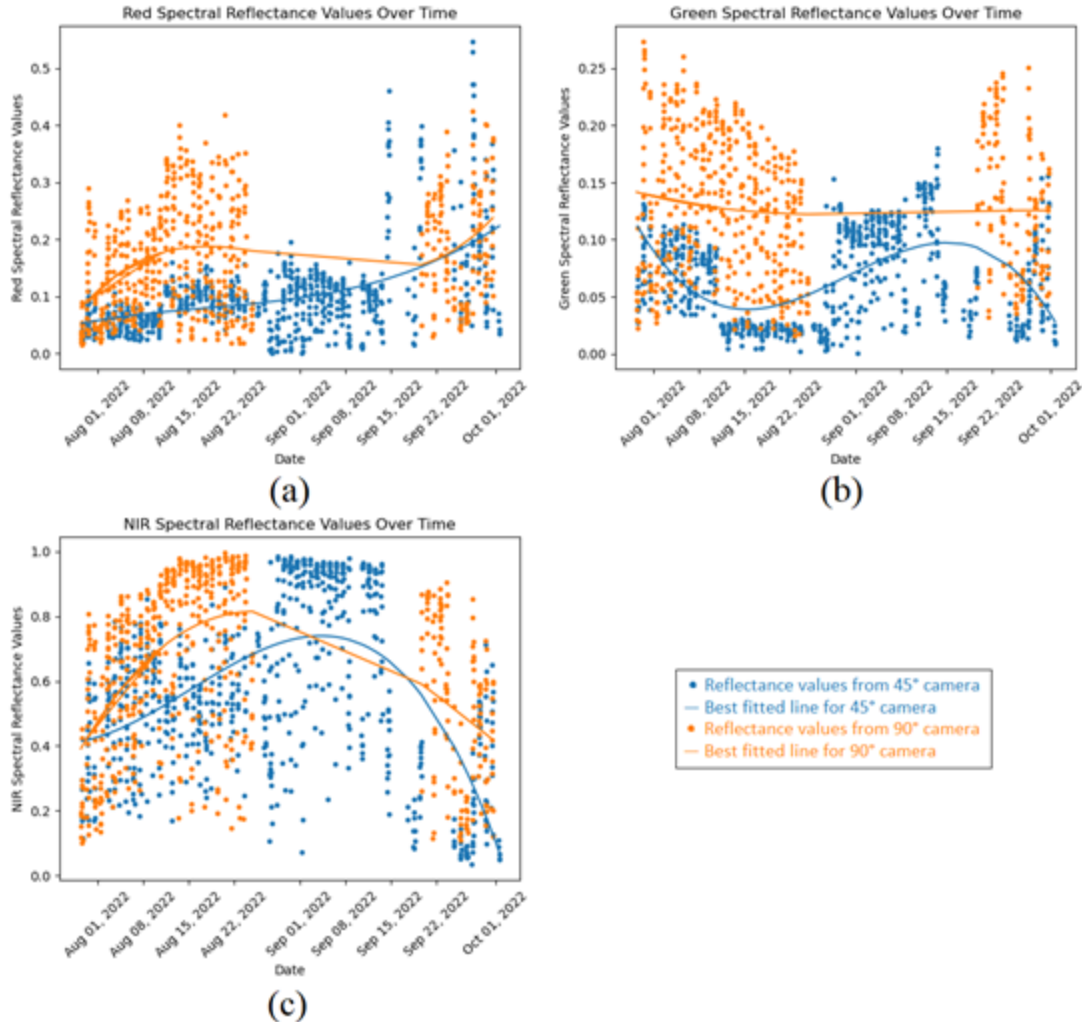


Figure 2.5: Change of spectral reflectance values in (a) Red, (b) Green, and (c) NIR bands over time for both 90° and 45° cameras. The dots represent mean spectral reflectance values for each leaf segment at a certain time, and the blue and orange lines are the best-fitted line among the points.

Figures 2.6-2.8 show how the vegetation indices change over time. The best-fitted line shows how the overall vegetation indices change over time among the crop canopies. Visually, there is no difference between the 90° and 45° angle cameras. The best-fitted lines for both cameras showed an approximate peak of NDVI value of 0.85, peak GNDVI value of 0.9, and peak SAVI value of 0.8. NDVI and SAVI reached their peak in mid-August, which falls in the R4-R5 stage, but on the other hand, GNDVI kept increasing up until late August, which falls in the R5-R6 stage (late August to September). Due to a system failure during the R6 stage, no images were captured.

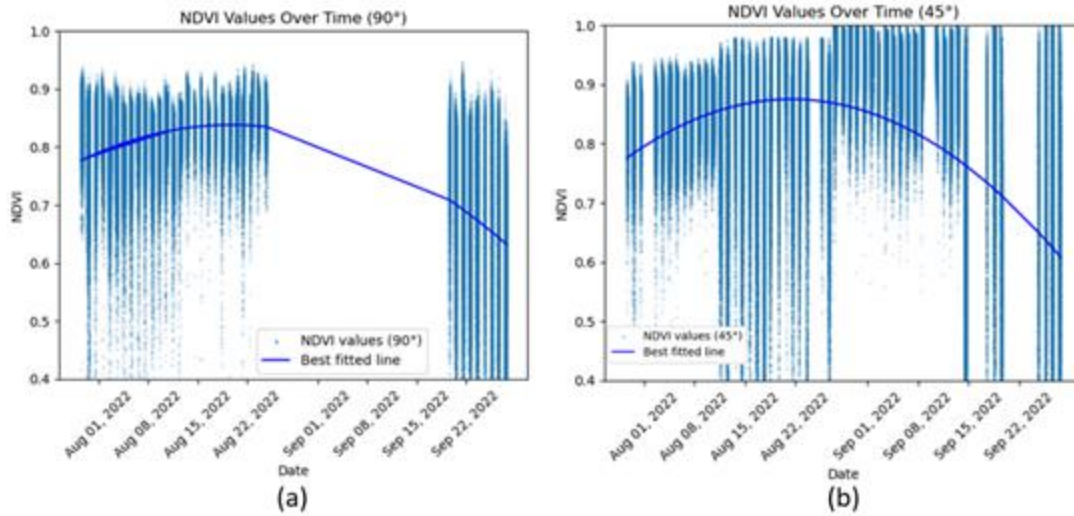


Figure 2.6: NDVI values over time (R4-7 stages): (a) 90° camera and (b) 45° camera. The blue dots represent mean NDVI values for each leaf segment over time, and the blue line is the best-fitted line for those points.

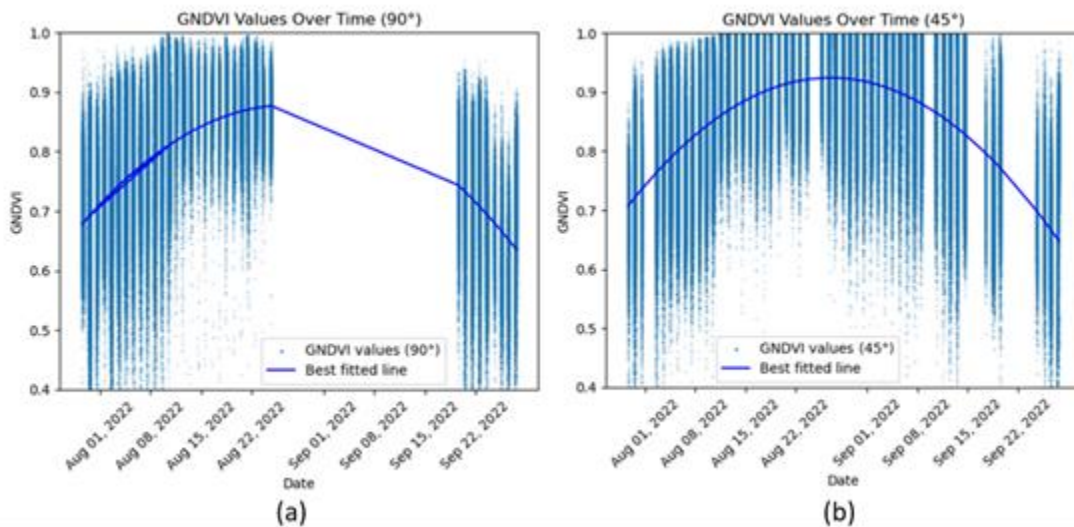


Figure 2.7: GNDVI values over time (R4-7 stages): (a) 90° camera and (b) 45° camera. The blue dots represent mean GNDVI values for each leaf segment over time, and the blue line is the best-fitted line for those points.

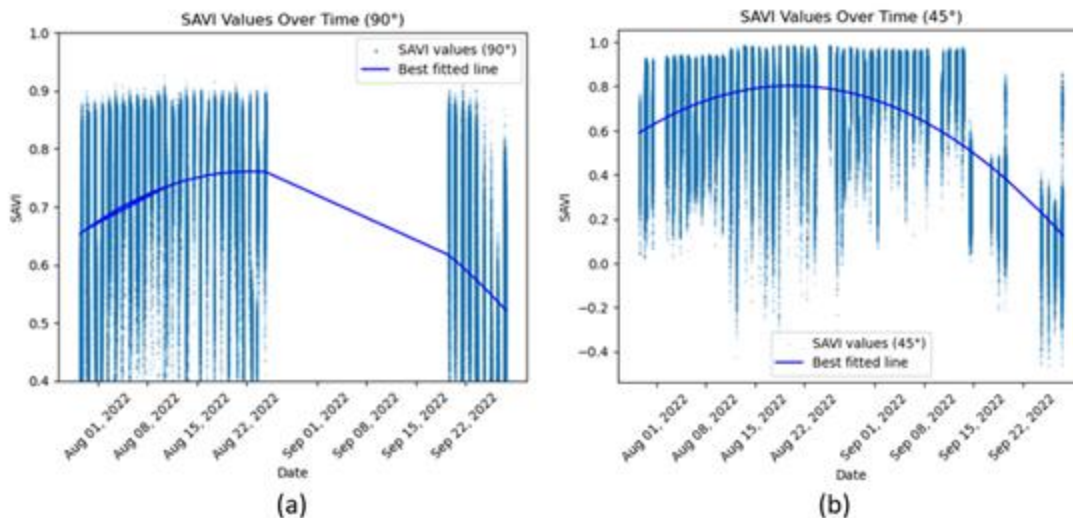


Figure 2.8: SAVI values over time (R4-7 stages): (a) 90° camera and (b) 45° camera. The blue dots represent mean SAVI values for each leaf segment over time, and the blue line is the best-fitted line for those points.

2.4 Discussion

The study selected the Mapir 3W RGN camera, which is a relatively low-cost camera with NIR band (around 400 USD). It is significantly lower compared to other spectrometers and sensors available in the market. For example, there are RedEdge-MX multispectral cameras by MicaSense (Measure), Sequoia multispectral cameras by Parrot (Aeromotus), etc., but they are very expensive and sophisticated cameras that are not suitable for general farmers (Barrows & Bulanon, 2017; Fensham & Fairfax, 2002; Omia et al., 2023; Raeva et al., 2018). On the other hand, low-cost digital commercial cameras are not sensitive to the NIR region of the electromagnetic spectrum and do not record data in three separate bands.

2.4.1 Optimized Camera Parameters

This study focused on optimizing the image-capturing procedure for Soybean health monitoring. Considering factors such as sensor selection, sensor orientation, ground area coverage, power supply, and automated image-capturing process, a comprehensive analysis was done to optimize the image-capturing workflow. The data capturing was initiated in the summer of 2021. After analyzing the performances, the workflow was improved in the summer of 2022.

In the summer of 2021, a solar panel with a power output of 6W and a lithium polymer battery with a capacity of 26.8 Ah were utilized to provide power to the camera setup. However, it was observed that during extended periods of cloudy weather lasting two to three consecutive days, the battery failed to receive sufficient charge, leading to an inadequate power supply for the camera and Raspberry Pi 4 Model B computer. Additionally, the region of Northwestern Ontario experiences low night-time temperatures, even during the summer season, with temperatures dropping to around 5°C. These colder temperatures further reduced the battery's capacity. Therefore, it was necessary to enhance the power capacity for the subsequent year in 2022. Accordingly, the battery capacity was increased to 80Ah, and the solar panel capacity was increased to 60W. This upgrade ensured that the camera setup could be powered for an extended duration of two to three days, even in the absence of sunlight due to cloud cover. This sustainable power setup enabled the system to operate autonomously throughout the entire Soybean growing season.

2.4.2 Camera orientation

Our findings indicate that both vertical (90°) and oblique (45°) camera orientations can provide accurate measurements of soybean health, with different benefits and limitations. For example, the classification results of images from the vertical camera, indicated that more pixels were overexposed than the other camera (Table 2.3). The vertical camera might capture more radiation reflected from the surface of the leaves, which leads to overexposure (Yue et al., 2018). On the other hand, a slower shutter speed will provide overexposed images unless the ISO changes accordingly (Sony Electronics Inc., 2019). There are no significant differences between the two cameras in terms of VIs (Figures 2.6-2.8). VIs are ratios of surface reflectance values of multiple bands designed to highlight distinct vegetation properties (Pasimeni et al., 2018). These ratios enhance the spectral characteristics of Soybean leaves in the image irrespective of image illumination (sun angle and viewing angle). Therefore, both cameras should provide similar results.

Some images were missing in the R6 stage due to a system failure. It was recovered, and therefore, images were available for R7. However, according to Vásquez et al., 2023, there was not much difference between spectral reflectance values of the R5 and R6 stages of Soybean. The Mapir

Survey 3W camera has an optional GPS to tag the camera exposure station location to the images, offering valuable assistance when working with various image analysis tools such as ENVI (NV5 Geospatial Solutions Inc., 2024), ESRI ArcGIS Pro (ESRI, 2023), and similar applications. We would recommend attaching the GPS to the camera in the future.

2.4.3 Operational Cost

The initial expenditure associated with the assembly of our experimental setup was around CA\$1707. However, it is imperative to underscore that this investment was specifically designed for research purposes. For the end users, primarily the farmers, the acquisition of the camera sensors constitutes the essential expenditure. The procurement of additional components remains optional. A singular camera unit suffices for the collection of remote sensing data related to the analysis of designated areas within soybean fields. Consequently, this strategic reduction in requisite hardware diminishes the operational costs significantly, from an initial outlay of seventeen hundred Canadian Dollars to a mere five hundred Canadian Dollars. This cost-effective approach not only ensures the accessibility of the technology to the end users but also underscores the potential for scalability and adaptability in diverse agricultural settings.

2.5 Conclusions

This study aimed to analyze the optimal properties and orientations of field cameras for assessing soybean health. Despite the abundance of research and scholarly publications about crop health monitoring utilizing Remotely Piloted Aircraft Systems (RPASs), aerial photography, and satellite technology, there remains a notable lack of comprehensive exploration regarding the potential and optimization of proximal field cameras. In this study, we tried to fill that gap by optimizing the image-capturing workflow using a proximal field camera.

An optimally designed structure and system were devised to establish field cameras to evaluate soybean health. We gained valuable insights throughout the optimization process, which led to notable advancements in the camera setup's design and performance. Besides that, a significant improvement was achieved in the power supply system, which now operates efficiently while ensuring an uninterrupted power source even in the event of consecutive cloudy weather conditions lasting two or three days. The image capturing process has been automated, minimizing the need

for human intervention or supervision during operation. Although regular field visits were conducted on a weekly basis to verify the system's functionality, no further manual interventions were necessary as the system consistently operated smoothly and as intended.

Typically, expensive, and sophisticated equipment can provide better results. However, considering end users as general farmers, it is necessary to optimize the cost of the entire camera setup. The Mapir Survey 3 W camera we chose for this setup is capable of capturing images in Red, Green, and Near Infrared, which were required. The materials used for the pole structure to mount the cameras are very cheap but sufficiently strong to withstand wind and rain. The entire setup was automated with a microcontroller system built with Raspberry Pi 4 Model B that does not require any external power but can take pictures all day.

Our findings show that the reflectance values obtained from the two camera orientations recorded higher values when captured by the vertical camera (90°). In both cases, a shutter speed of 1/125 seconds was set. However, while this camera setting proved effective for the oblique camera orientation (45°), it resulted in overexposure in the images captured by the vertical camera (90°). Consequently, it is recommended to adjust the camera shutter speed to a higher value (corresponding to a lower exposure time) specifically for the vertical camera orientation (90°) to mitigate the issue of overexposure.

Vegetation indices do not seem to be affected much by the camera properties because they are the ratio of different band reflectance values; however, the accuracy of the vegetation indices can be affected by the spectral performance of the camera, which can affect the quality of the reflectance values used to calculate the indices.

Overall, the optimization of the soybean image-capturing procedure through the refinement of the power supply, camera settings, and the inclusion of GPS georeferencing capabilities has significantly improved the effectiveness and reliability of the camera setup. These advancements contribute to more accurate assessments of soybean health and enable informed decision-making in crop management, all while considering cost efficiency.

Chapter 3: Monitoring Soybean Leaf Chlorophyll Content Using Low-Cost Remote Sensor

3.1 Introduction

Soybean is an extremely valuable crop globally due to its versatility and wide range of uses (Pagano & Miransari, 2016). For instance, it is one of the richest proteins that is used in people's and animal diets. Many industries use soybean oil as an ingredient in their products, such as paint, wood veneer adhesives, linoleum backing, and fire extinguisher fluids (Johnson & Myers, 1995). Hence, this is a vital crop, and monitoring soybean health is crucial for farmers to maximize its yields and quality. Annually, about 2 million acres of Soybeans are cultivated in Ontario, Canada, for about \$4 billion market size (Ministry of Agriculture, Food and Rural Affairs, 2021). However, the industry is expected to grow over the next five years time (Ministry of Agriculture, Food and Rural Affairs, 2021). Considering the significant impact and extensive cultivation of Soybeans in Canada, closely monitoring the crop's health became crucial for ensuring maximizing the yield.

Traditional crop health monitoring methods are usually destructive, require lots of experience, and are unsuitable for large-scale farms (Omia et al., 2023). Remote sensing plays a vital role in reducing the farmers' workload and providing valuable information to farmers to monitor and manage their crops. Remote sensing has been used to detect soybean diseases, allowing site-specific management to reduce pesticide use at the farm level (Omia et al., 2023). For example, a study in Brazil aimed to quantify the reduction of pesticides applied to soybean and maize crops at various stages of the production cycle by using a precision spraying control system based on real-time sensors (Zanin et al., 2022). The system allowed for applying pesticides only where necessary, thus reducing the volume of pesticides used and potentially lessening environmental contamination. Further, Omnia et al., 2023 discussed the use of various remote sensors at the farm level and, thus, the reduced workload of farmers (Omia et al., 2023). However, the most common remote sensing data source for Soybean mapping and monitoring are satellite images and images from Remotely Piloted Aircraft Systems (RPAS) (Eugenio et al., 2020; Fathi & Shah-Hosseini, 2023). There are advantages and disadvantages associated with each sensor system. For instance,

usually, the affordable and most accessible satellite images have a low spatial resolution, and their revisit time is almost two weeks (Borotkanych, 2022; Toth & Józkw, 2016). They also require expert knowledge to extract useful information. Some remote sensing options provide instantaneous results, for instance, field spectrometers, but the associated cost is high (Malvern Panalytical Inc., 2024; VertMarkets, 2021). Also, the images should be capable of detecting parameters that indicate the health of vegetation.

There are several parameters that can be used to analyze the health of the crops directly or indirectly using remote sensing methods such as canopy chlorophyll, nitrogen, phosphorus, and potassium contents (Kganyago et al., 2021), soil moisture (Ahmad et al., 2010), soil nutrient levels (Samreen et al., 2023), and disease symptoms (Shahi et al., 2023). The estimation of leaf chlorophyll content (LCC) in soybeans is a critical aspect of precision agriculture, particularly given the unique nitrogen-fixing ability of legumes like soybeans. Soybeans, as legumes, have the capacity to fix atmospheric nitrogen (N) through symbiotic relationships with rhizobia bacteria, which reduces the necessity for external nitrogen application (Mabrouk et al., 2018; Mylona et al., 1995). This biological process significantly influences the nitrogen dynamics within the soil and the plant (Mabrouk et al., 2018). This biological process can be interrupted by several factors, such as atmospheric vapor pressure deficit (VPD) and precipitation during early reproductive growth (R1–R4 stages), sowing date, drought stress during seed filling (R5–R6), soil cation exchange capacity (CEC), and soil sulfate concentration before sowing (de Borja Reis et al., 2021).

Estimating leaf chlorophyll content (LCC) can help in detecting problems associated with the nitrogen fixation process because LCC is closely related to the plant's nitrogen levels, as nitrogen is a crucial component in chlorophyll molecules and combined protein complexes (Y. Zhang et al., 2020). A healthy chlorophyll concentration indicates a well-functioning nitrogen fixation process, as chlorophyll plays a pivotal role in photosynthesis, the process through which plants convert light energy into chemical energy, utilizing nitrogen in the process (Evans & Clarke, 2019). This makes the monitoring of leaf chlorophyll content an essential indicator not only for plant health but also for nitrogen utilization efficiency.

Multispectral and hyperspectral images acquired using an RPAS can be used to analyze leaf chlorophyll content and canopy cover (Z.Zhang & Zhu, 2023). They provide high spatial, spectral,

and temporal resolutions. Currently, one of the low-cost, multispectral cameras in the market is the Mapir Survey 3W camera, which is an alternative to field measurements to monitor agriculture crops (Mapir Camera, 2021). So far, limited studies have used this camera for agricultural applications. However, (Vásquez et al., 2023) used one of the Mapir Survey 3W cameras (orange, cyan and NIR bands) to develop a new vegetation index to assess soybean growth dynamics.

Vegetation indices combine spectral reflectance of two or more bands of an image to emphasize vegetation properties. They are straightforward yet effective for the quantitative and qualitative assessment of vegetation cover, health, and growth dynamics (Xue & Su, 2017). Normalized Difference Vegetation Index (NDVI) is the most widely used vegetation index that measures the difference between near-infrared (NIR), where vegetation strongly reflects, and red (R), which vegetation absorbs. It is one of the most popular vegetation indices used for detecting plant health status. However, the NDVI value saturates when it approaches its upper limit (close to 1) due to high biomass in dense vegetation. The Leaf Area Index (LAI) of a plant is a dimensionless quantity that represents the one-sided green leaf area per unit of ground surface area (Liang & Wang, 2020). In other words, a higher LAI indicates denser green vegetation. When the LAI is high, NDVI tends to plateau or saturate (Wang et al., 2016). NDVI does not increase linearly with increasing vegetation density when the plants reach their matured period (Aklilu Tesfaye & Gessesse Awoke, 2021). There are some other vegetation indices, such as Simple Ratio (SR) and Transformed Vegetation Index (TVI), that use the primary bands of Red, Green, and Near-infrared (Aklilu Tesfaye & Gessesse Awoke, 2021); thus, the issue related to the spectral behavior of red and NIR that identified with NDVI still persists with these indices. Green Normalized Difference Vegetation Index (GNDVI) is a vegetation that uses the primary bands of Green and Near Infrared and reaches saturation later than other indices (Gitelson et al., 1996). So, GNDVI was considered a better predictor index for the prediction of leaf chlorophylls for dense vegetation like Soybean.

Gaitán et al., 2013 evaluated the performance of several remote sensing indices to predict the spatial variability of ecosystem structure and function. Pereira et al., 2023 found that while vegetation indices were useful, their applications were limited by the expense of the equipment, technical hurdles, interpretational challenges, and data quality issues. Stamford et al., 2023 developed a low-cost NDVI imaging system for assessing plant health, demonstrating NDVI's application in plant phenotyping and health assessment. One of their limitations is the camera setup

they have used. The off-the-shelf modified cameras used in their system can affect the accuracy of the NDVI values obtained. Furthermore, the calibration method used is complex and requires expert knowledge. So, a much simpler system is needed to make it more viable for end users. In the scoping study (Chapter 2), we explored the affordable, reliable, and robust set of equipment, set-up parameters, and image-capturing process for Soybeans. A Mapir Survey 3W (Mapir Camera, 2024) camera sensitive to red-NIR of the electromagnetic spectrum acquiring images at about 6 feet in height could be an ideal solution for monitoring Soybeans.

The need for software applications to monitor crop health is underscored by several critical factors that enhance agricultural productivity and sustainability. These applications leverage advanced technologies such as remote sensing, data analytics, and artificial intelligence to provide precise, real-time insights into crop conditions, enabling more informed decision-making in agricultural management (Omiya et al., 2023). In order to visualize the LCC of test plots, a prototype application was necessary to be developed. There are many existing sophisticated crop health monitoring software in the market. For instance, Crop Monitoring (EOS Data Analytics Inc., 2024) is a very advanced satellite-based crop health monitoring application. There are other software such as Climate FieldView (Climate LLC, 2023), CropX (CropX Inc., 2024), etc. The problem with most of the existing software is that it depends on satellite data, which might be ideal for large-scale farms but not very useful for small-scale farms because of the low spatial and temporal resolution and high operational cost (Omiya et al., 2023). This study proposed a prototype, cost-effective crop monitoring system that might be suitable for small-scale farms too.

The main aim of the study in this chapter was to analyze the images obtained from field cameras for site-specific variations. The specific objectives were to (i) set up the Mapir Survey 3W camera in the field for imaging; (ii) determine the relationship between the measured leaf chlorophyll content and remotely acquired spectral information; (iii) map the spatial distribution of leaf chlorophyll using the spectral information over the study area; and (iv) develop a prototype web application for the end users to get the leaf chlorophyll content.

3.2 Data and Method

3.2.1 Study area and data collection

The study was conducted at the Lakehead University Agricultural Research Station (LUARS) located in Thunder Bay, Ontario, Canada (48.3052° N, 89.3882° W) (Figure 3.1). Thunder Bay has a humid continental climate in Northwestern Ontario (Weather Spark). The area experiences four distinct seasons, with warm summers and cold winters. Thunder Bay has an average annual temperature of 3.2°C, with the warmest month being July, with an average temperature of 17.4°C, and the coldest month being January, with an average temperature of -13.6°C (Ahmed et al., 2014). The experimental soybean plots are marked in Figure 3.1. The Soybean was seeded on May 18, 2023, in a grid block pattern, with each plot sizing about 1.8 m x 3.5 m and a 0.33 m buffer zone between each plot on a total area of 29 m x 21 m. In late August, just before harvesting, a deer grazed and trampled the entire experimental field. Hence, the harvest information was not available.

A Mapir Survey3W (RGN) camera that is sensitive to red, green, and near-infrared regions of the electromagnetic spectrum was used to collect data. The camera was set up according to the specifications confirmed by the scoping study of this research (details were outlined in the Chapter 2 of this thesis). The images were acquired daily from 9 am to 5 pm throughout the growing season (June to August). Images of the calibration panel of the camera were obtained frequently to convert DN values into spectral reflectance values. Table 3.1 shows the central wavelength of each band. The bandwidth of a single band is 15nm. The camera was mounted on a PVC frame looking straight down (90°) at a height of about 152 cm. The shutter speed was set to 1/250s, the aperture was set to f/2.8, and ISO was set to 100.

Table 3.1: Spectral resolution of MAPIR Survey 3W Camera (MAPIR CAMERA, 2023).

Spectral Band	Central Wavelength (nm)
Red	660
Green	550
Near Infrared	850

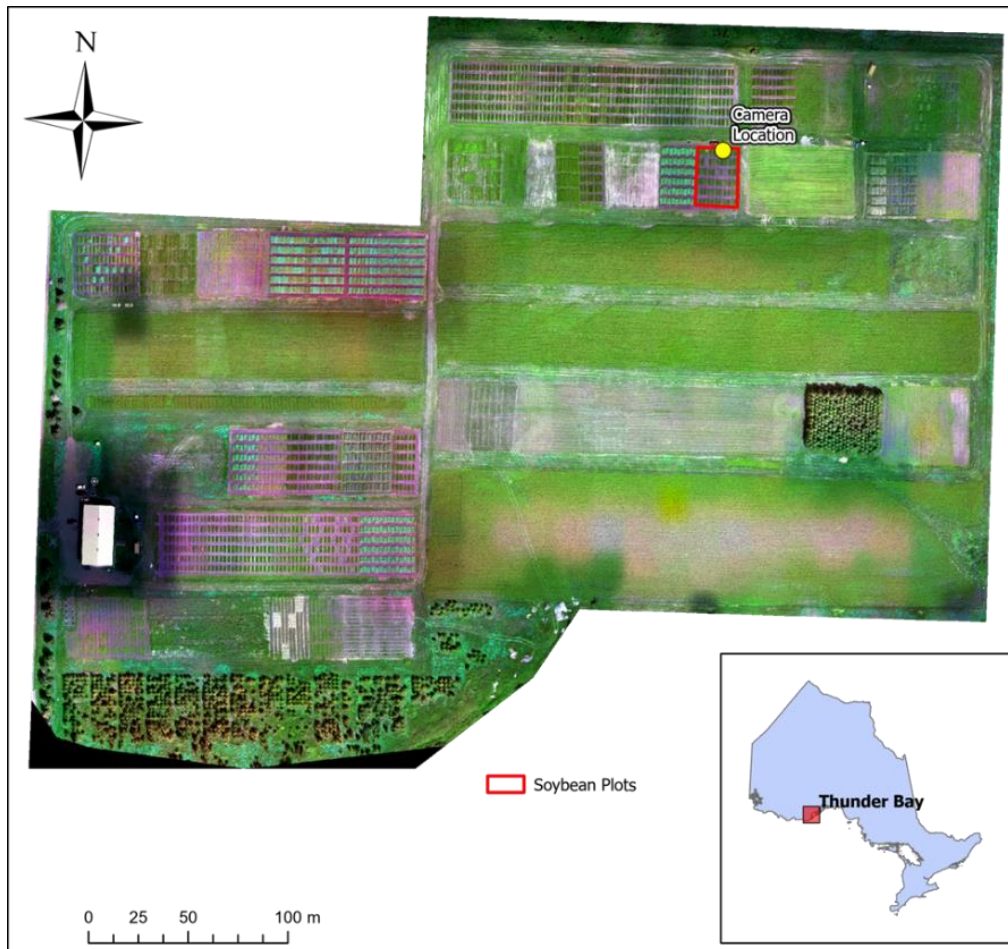


Figure 3.1: A map of the Lakehead University Agriculture Research Station, Thunder Bay, Ontario, Canada. The location of the camera (yellow points) and a soybean plot (red polygon) are shown on the map.

The camera setup was automated to capture images, but images were downloaded manually. Field visits were conducted every 7-10 days (depending on the weather and availability of the researcher) to collect sample data. Leaf Chlorophyll Concentration ($\mu\text{mol m}^{-2}$) was measured on each field visit using an Apogee chlorophyll meter (model: MC-100) (Apogee Instruments, 2024). There were approximately 220-250 plants per plot. The average of five readings per leaf was considered as one leaf's chlorophyll content. Around 29-35 random leaves were measured at each plot in every field visit.

3.2.2 Data processing and analysis

Images were sorted for days when Chlorophyll data were collected and calibrated to obtain spectral reflectance using Mapir Camera Control software (Mapir Camera, 2024). Then, the images were segmented into individual leaves. The most suitable image segmentation method for Soybean images was identified in the scoping study. A Python script was written to divide the entire image into smaller blocks images (100 x 100 pixels), allowing a maximum of four leaves in one block. The watershed algorithm (Kornilov & Safonov, 2018) was used on each block, and block results were combined later to obtain the whole individual leaf segmented image.

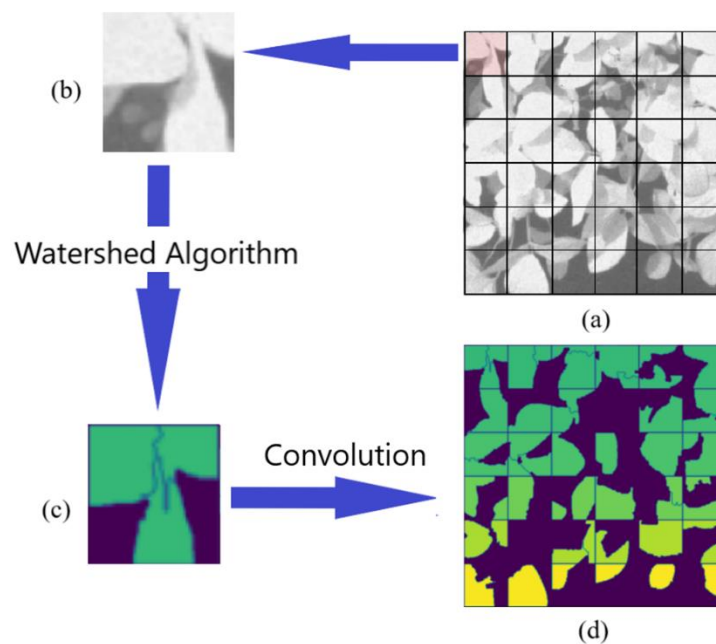


Figure 3.2: Individual leaf segment using the watershed algorithm. (a) the whole image divided into smaller blocks of windows; (b) shows the zoomed area over a small block; (c) shows the segmented smaller blocks using the watershed algorithm; (d) shows the final constructed individually segmented image after convolution.

Extracting leaf chlorophyll content

The Green Normalized Difference Vegetation Index (GNDVI) is proposed as an alternative to NDVI to overcome the saturation problem. GNDVI uses the green (G) band instead of the red band and is calculated as follows (da Silva et al., 2020).

$$GNDVI = \frac{NIR - G}{NIR + G} \quad (1)$$

It can be used at later stages of crop development, as it saturates later than NDVI, providing a more linear response to increasing biomass even at higher LAI levels (Prabhakara et al., 2015). For this study, GNDVI was selected for analysis, considering the availability of three bands from the camera and the saturation effect.

GNDVI was calculated for each image, and the mean values were extracted for each leaf segment using a Python script. A table was created at the time of image acquisition. A relationship function between GNDVI and time (T), where T is expressed as the number of days from seeding, is calculated using piecewise linear regression using Python's scikit learn library (Scikit-Learn, 2007).

So, the whole GNDVI variation can be written as a function of time,

$$GNDVI = F(T) \quad (2)$$

A similar relationship between the ground truth data (LCC) and time (T) can be established.

$$LCC = G(T) \quad (3)$$

Both LCC and GNDVI are functions of time. By rearranging Equations (2) and (3), the equation (4) can be derived. Equation (4) shows the relation between LCC and GNDVI.

$$LCC = G(F^{-1}(GNDVI)) \quad (4)$$

By looking at the data pattern in Figures 3.3 and 3.4, it seemed like the relationships could be expressed best as a quadratic function; but the inverse of a quadratic function provided two possible solutions. Hence, a piecewise linear equation was used to establish a linear relation between GNDVI and time (T). The whole Soybean season was divided into three stages: (i) the growing stage (first 65 days since seeding), (ii) the matured stage (next 30 days), and (iii) the production stage (next remaining days), which lasts till harvest. So, three different linear equations were created for each stage.

There are several statistical tests that compare two distributions to see if the actual and predicted LCC vs. time distributions are alike or different. Hence, the robustness of the model was assessed using a statistical test: Kolmogorov–Smirnov test. The field samples of LCC (ground truth LCC) over time and the predicted LCC over time were compared. The null hypothesis was that there is no difference between the two LCC distributions (Predicted LCC over time and Actual LCC over time). The resultant p-value and KS statistics were noted.

3.2.3 Building the prototype web application

Finally, a prototype web application was developed so that end users could experience the established relationship between LCC and GNDVI. A Django framework (Django Software Foundation) is used to build the Representational State Transfer (REST) Application Program Interface (API) that takes the calibrated image with some other parameters and returns the LCC distribution image as a response. The interface was straightforward. Users can upload their images with some field attributes (seeding date, image capturing date, and upload an image). The “Analyze” button in the interface will initiate performing the background calculation and produce results for the user. The resultant image shows the spatial distribution of LCC at the time of image capturing.

3.3 Results

In the segmented images, about 383-750 leaf segments were obtained for each image. The mean GNDVI value was recorded for each leaf segment as a corresponding row in a Comma Separated Value (CSV) file.

Figure 3.3 (a) shows the change in GNDVI over time. GNDVI increased from July to mid-August, plateaued for about 10-12 days, and decreased at the end of August. Figure 3.3 (b) explains the linear relationship between GNDVI (Y axis) and No. of days from seeding (X axis) for three different growing stages identified (Growing Stage, Matured Stage, and Production Stage). In this figure, each of the blue data points represents the GNDVI value of each of the leaf segments.

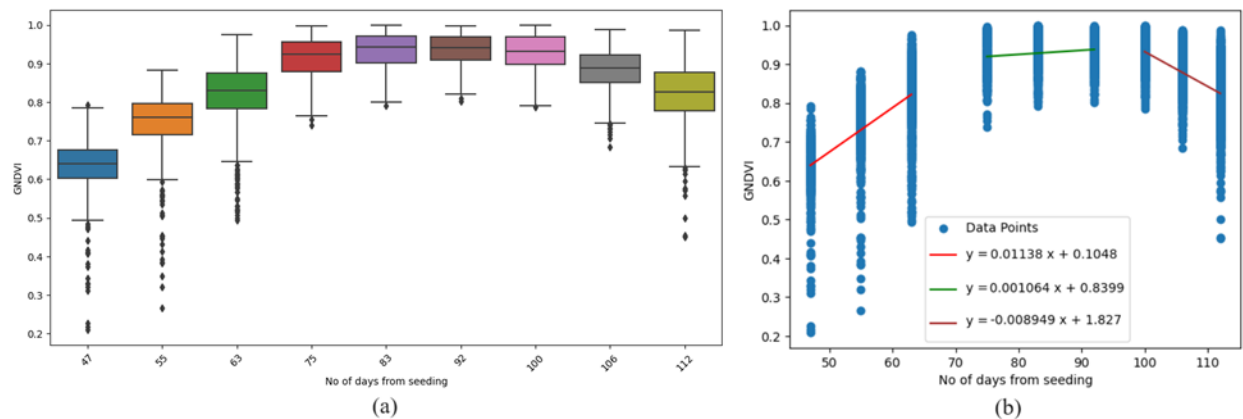


Figure 3.3: Geen Normalized Difference Vegetation Index (GNDVI) change over time; (a) GNDVI changes with respect to no. of days from seeding; (b) GNDVI values overlayed with the best-fitted piecewise linear regression models.

Figure 3.4 (a) shows how the leaf chlorophyll content changed over time. Leaf chlorophyll content didn't change much in the initial growing season, but after mid-July, it was increased. After the mature period, there was a downward trend when the crops were getting prepared for harvesting. This is evidenced in Figure 3.4 (b), which superimposed the best-fitted functions with the LCC and no. of days from seeding.

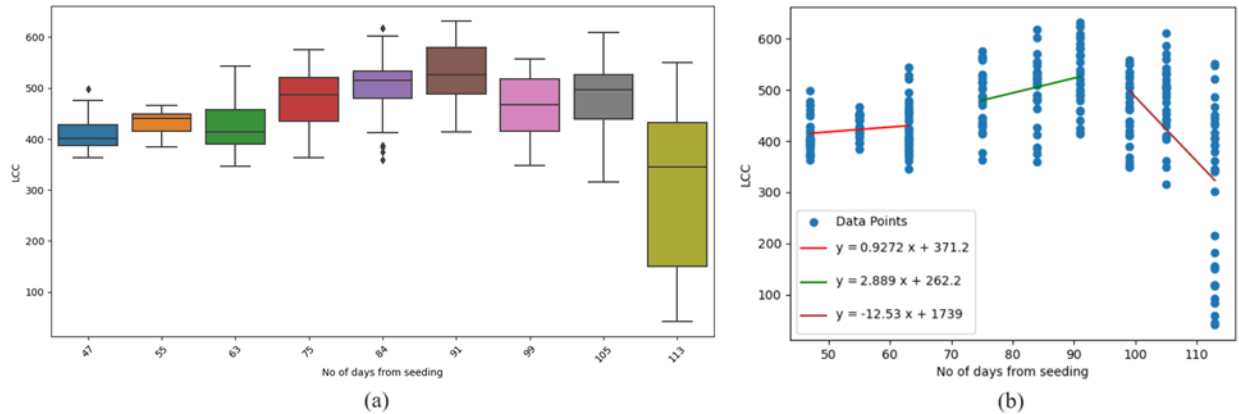


Figure 3.4: Leaf Chlorophyll Content (LCC) ($\mu\text{mol m}^{-2}$) change over time; (a) LCC changes with respect to no. of days from seeding; (b) LCC values overlaid with the best-fitted piecewise linear regression models.

After rearranging the piecewise linear equations mentioned in Figures 3.3 (b) and 3.4 (b), the relationship between LCC and GNDVI was established. The Equation (5) shows the derived relationships for three growing stages.

$$LCC = \begin{cases} 286.478 \times GNDVI + 242.661 & (\text{If } T < 65) \\ 2006.3 \times GNDVI - 1359.3 & (\text{If } T < 95) \\ 1400.16 \times GNDVI + 819.086 & (\text{If } T \geq 95) \end{cases} \quad (5)$$

where T is the number of days from the seeding date.

The result of the Kolmogorov–Smirnov (KS statistics) test was not statistically significant (p-value = 0.12). The KS statistic value was 0.0718.

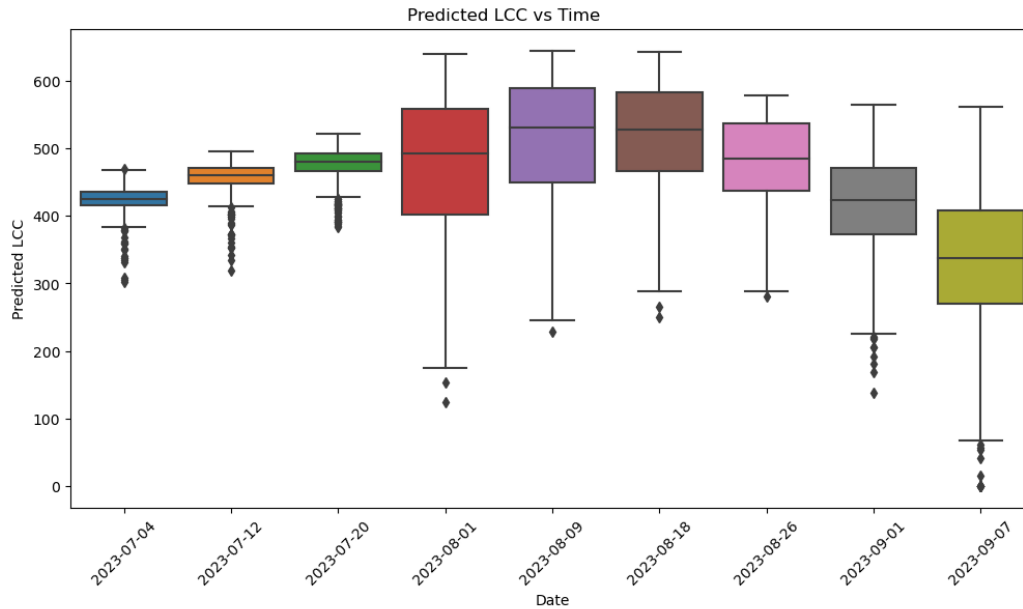


Figure 3.5: Predicted Leaf Chlorophyll Concentration ($\mu\text{mol m}^{-2}$) change over time derived using the equation (5).

Figure 3.6 shows the spatial distribution of chlorophyll at the previously considered growing stages. Figure 3.6 (a) represents the initial stage. At that time, leaves were not fully grown, and the soil was exposed to the images and shown in the red-orange shade (the lowest values). Figure 3.6 (b) corresponds to the matured stage (after 84 days of seeding) and the leaves were healthy and indicated the highest LCC. (dark green color). The Figure 3.6 (c) was prepared for the production stage, by then, leaves were turning to brown and LCC levels were decreased.

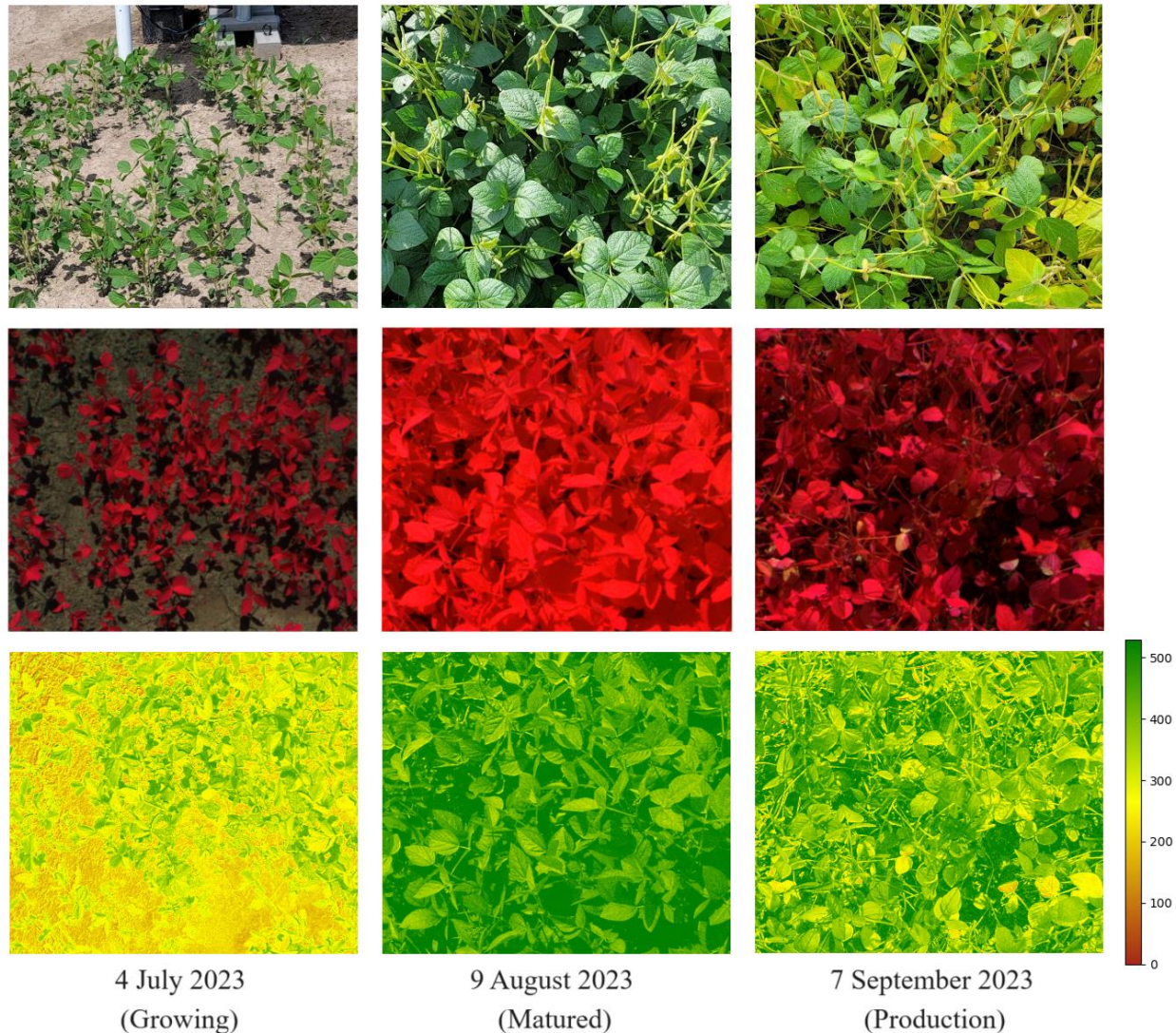
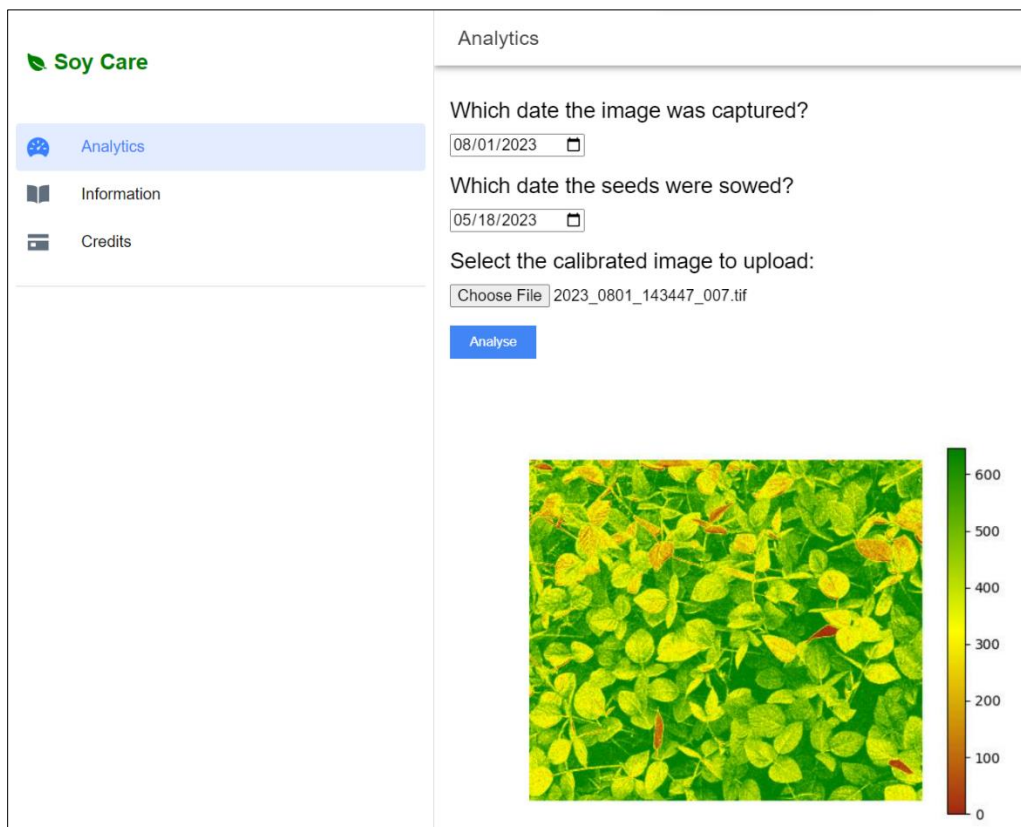


Figure 3.6: Top row: field photos captured (with a Samsung Note 20 Phone Camera) on the same date the corresponding RGN images were captured; Middle row: Corresponding RGN image; Bottom row: Corresponding chlorophyll distribution image.

The developed prototype application titled “Soy Care” features an intuitive, web-based user interface designed to facilitate soybean leaf chlorophyll monitoring. The interface is divided into several sections, each serving a specific purpose (Figure 3.7). A navigation bar provides access to different sections of the application, including “Analytics,” “Information,” and “Credits”. While the “Information” section contains some background information about what this application does and what the results interpret, the main functionality of this application is under the “Analytics” section.

Clicking on the “Analytics” section a form appears. Users can specify the date when the image was captured and the date when the seeds were sowed. These date inputs allow the application to contextualize the data and provide relevant analysis. The application then takes the calibrated image as input. If all the inputs were given correctly, the user can click the Analyze button and wait until the result image returns.

The input data is processed in the backend server and returned. The application then shows the output chlorophyll distribution image and displays below the upload form. The application is now in testing phase and the url: <https://samiul-lakehead.github.io/soy-care/>



The screenshot displays the 'Soy Care' web application interface. On the left is a navigation sidebar with 'Analytics' selected. The main content area is titled 'Analytics' and contains a form with the following elements:

- Question: "Which date the image was captured?" with a date input field showing "08/01/2023".
- Question: "Which date the seeds were sowed?" with a date input field showing "05/18/2023".
- Text: "Select the calibrated image to upload:"
- File selection: A "Choose File" button followed by the filename "2023_0801_143447_007.tif".
- Action: A blue "Analyse" button.

Below the form, the application displays a heatmap of a soybean field. The heatmap uses a color scale from 0 (dark red) to 600 (dark green) to represent chlorophyll content. A vertical color bar on the right side of the heatmap provides the scale, with numerical markers at 0, 100, 200, 300, 400, 500, and 600.

Figure 3.7: An example of the web application interface to map the spatial distribution of leaf chlorophyll content.

3.4 Discussion

In this study, leaf chlorophyll content was selected as an indicator of plant health instead of canopy chlorophyll content mainly due to the capability of the proposed imaging system. The camera setup is capable of acquiring high spatial and temporal resolution images over the growing season as opposed to using satellite images. For example, the limited spatial and temporal resolution of satellite imagery does not provide information up to a leaf level (Borotkanych, 2022; Suwanprasit & Srichai, 2012). This identifies the advantages of the proposed system for instance, the capability to capture variations within each plant, making it more precise and allow farmers to treat them individually. In addition, the end users don't need an expensive setup to acquire this information.

The study selected GNDVI to map the spatial distribution of LCC over time. Though NDVI is a more widely used vegetation index, it has a major drawback. NDVI reaches a saturation point when the biomass gets denser (Aklilu Tesfaye & Gessesse Awoke, 2021). There are other alternative indices as well. For instance, the Soil Adjusted Vegetation Index (SAVI) uses the same input bands as NDVI but takes an extra input parameter that varies on the soil adjustment factor, which also depends on vegetation cover (da Silva et al., 2020). There are other vegetation indices such as Simple Ratio, Transformed Vegetation Index, GNDVI, etc. Among them, GNDVI is selected because it is more useful for plant monitoring as it minimizes the limitations associated with saturation (Mangewa et al., 2022), and it is calculated using the input bands that the camera used in this study (Mapir Survey 3W) can capture and does not depend on any other parameters like soil adjustment factors.

When modeling the relationship between LCC (field samples) change over time and corresponding GNDVI values over time, quadratic equations fit the data best (Finnan et al., 1997). However, the inverse of the quadratic didn't work well within this context. The process of inverse function does not allow the use of quadratic function. Quadratic functions are many-to-one mapping, and the inverse of many-to-one mapping is a one-to-many mapping, and a one-to-many mapping is not a function (Mathspace, 2022). The best way to establish the relation between LCC vs. time, GNDVI vs. time, and LCC vs. GNDVI is to use a piecewise linear equation that depends on time. This allows us to calculate an inverse function because all linear equations are one-to-one mapping, and the inverse of a one-to-one mapping is another one-to-one function.

Since the p-value was not statistically significant and the KS statistic was 0.07, it can be concluded that these two datasets were similar in values. The smaller KS statistics and value and higher p-value indicate that the compared distributions are very similar (Karson, 1968).

The spatial distribution of LCC values yielded noteworthy results across three distinct stages. For example, leaves at the top level exhibited reduced LCC, while those positioned lower displayed elevated LCC values. This observation aligns with the expected pattern, as newly emerged leaves at the top may possess lower chlorophyll content compared to mature leaves situated at lower levels of the plant canopy (Khan et al., 2018; ŠEsták, 1963). The estimated LCC change over time shows a lower chlorophyll at the beginning of the season, reaches a peak, and when it ages to harvesting, the leaves lose chlorophyll and turn yellow. This finding matches the chlorophyll dynamics explored in a study by Finnan et al., 1997.

The proposed linear model is now hosted on a website. The application has an intuitive, web-based user interface that makes it easy for farmers to input data, view results, and make decisions based on the results without requiring extensive technical skills or training. Compared to more sophisticated precision agriculture software packages like Crop Monitoring (EOS Data Analytics Inc., 2024), which can cost thousands of dollars per year, the application provides an affordable option built specifically to the needs and constraints of small and medium-sized soybean farms in the region.

3.4.1 Limitations and further recommendations

Firstly, the current methodology relies on the Mapir Camera Control software (Mapir Camera, 2024) for calibrating raw images and obtaining reflectance data. Although this software is user-friendly and well-documented, integrating the calibration process directly into the web application could streamline the workflow and reduce the technical burden on end-users. Collaborating with Mapir Camera to develop a public API for image calibration could be a valuable avenue for future work.

Secondly, the spectral bands available in the Mapir Survey 3W camera limit the range of vegetation indices that can be explored. While GNDVI has proven effective for minimizing saturation effects and capturing LCC dynamics, incorporating additional bands like Orange and Cyan could enable

the use of more advanced indices like NDRE and MSAVI. These indices have shown promise in assessing soybean growth dynamics (Vásquez et al., 2023) and could potentially improve the accuracy and sensitivity of the LCC estimation model. Investigating the use of multi-spectral cameras with a wider range of bands is an important direction for future research.

Another improvement could be in the use of growing degree days as a common variable related to LCC and GNDVI. The use of the number of days since seeding might make the model location-specific and not universally applicable. Growing Degree Days, which incorporates temperature data (Neild & Seeley, 1977), could make the relation more site-independent.

Finally, there is significant scope to expand the functionality and decision support capabilities of the web application. Integrating features for storing past plot health information, conducting time-series analyses, and suggesting appropriate management interventions based on the LCC estimates could greatly enhance the value of the tool for farmers. Developing these additional modules would require close collaboration with agronomic experts and end-users to ensure that the system meets the practical needs and constraints of soybean production in the region.

3.5 Conclusions

The study developed a cost-effective, remote sensing-based system for monitoring soybean leaf chlorophyll content (LCC) using the Mapir Survey 3W camera sensor. By selecting GNDVI as a predictor of LCC and establishing a piecewise linear regression model, the research demonstrated a strong relationship between the vegetation index and the key crop health parameter. The robustness of the model was confirmed through a Kolmogorov-Smirnov (KS) statistic test, which showed no statistically significant difference between the predicted and ground truth LCC distributions.

The results indicated a significant relationship between the vegetation indices derived from the camera data and the soybean health parameters. The integration of the LCC estimation model into a user-friendly web application highlights the practical potential of this approach for enabling precision agriculture practices among soybean farmers in Northwestern Ontario. By providing an affordable and accessible tool for monitoring crop health at a fine spatial and temporal resolution,

this study contributes to the development of more sustainable and efficient farming practices in the region.

In conclusion, the study underscores the importance of developing accessible remote sensing tools for farmers and highlights the potential of such technology to revolutionize crop health monitoring. Future research could focus on refining the data analysis methods, exploring the use of additional vegetation indices, and expanding the study to include other crops and environmental conditions.

Chapter 4: Conclusions and Recommendations for Future Research

4.1 Low-cost Remote Sensing System for Soybean Monitoring

This thesis explored the potential of using a remote sensing-based precision agriculture system for monitoring soybeans in Northwestern Ontario. Specifically, it sought to answer three key research questions: (a) What are the optimal properties and orientation of proximal field cameras for capturing high-quality images of soybean canopies? (b) What is the relationship between remotely sensed data and leaf chlorophyll content that can be used to model the spatial distribution of leaf chlorophyll content in the test plots? (c) How to build a prototype, user-friendly software application to deliver useful information to end users?

Chapter 2 investigated the optimal camera specifications and mounting configurations for monitoring soybean canopies, finding that low-cost Mapir Survey 3W cameras mounted at approximately 6 feet height provided the best balance of image quality, coverage, and cost. It also investigated the camera orientation between vertical (90°) angle and (45°) camera orientation. It was found that the vertical camera captured more sunlight than the oblique orientation. To further optimize the operational cost, a polyvinyl chloride (PVC) material was recommended to build the frame for mounting the camera to ensure the proper rigidity of the setup. A Raspberry Pi 4 Model B controller is recommended for automating the image-capturing procedure, considering its potential and low cost. Though the experimental setup costs around CA\$1700 in practical scenarios, it is just the cost of the cameras that the end users need to bear, which is about CA\$500.

Chapter 3 investigated the relationship between the Green Normalized Difference Vegetation Index (GNDVI) and Leaf Chlorophyll Content (LCC). A piecewise linear regression model was developed to explain the relationship between LCC and GNDVI. The test results indicated a strong relationship between the two variables. From the predicted chlorophyll distribution images, it was observed that top-level leaves had less chlorophyll than lower-level leaves, and chlorophyll changes over time show lower chlorophyll in the initial stages, peak at the matured stages, and again a fall in chlorophyll values in the later stages. A web-based prototype application was

developed using the established model so that the end users can use the application to get site-specific information about crops and take measurements accordingly.

The integrated precision agriculture system developed in this thesis offers several key contributions and benefits. First, it demonstrates the feasibility and value of using low-cost remote sensing technologies for soybean monitoring in the challenging growing conditions of Northwestern Ontario. Second, it provides new insights into the relationships between remotely sensed plant traits and agronomic outcomes, which can inform more targeted and timely management interventions. Third, it translates these research findings into a practical, user-friendly decision support tool that can help farmers optimize input use, reduce costs, and improve yields and sustainability.

By tailoring the system to the specific needs and constraints of soybean production in this region, the research fills some gaps in the precision agriculture literature and offers a promising pathway for enhancing the productivity and resilience of local farming systems. The developed system has the potential to revolutionize soybean farming in Northwestern Ontario by providing farmers with real-time, actionable insights into crop health and management needs.

4.2 Limitations and Future Recommendations

It is important to acknowledge the limitations of this study and the need for further research. The findings are based on two growing seasons (2022 and 2023) and a limited number of field sites, so additional testing across multiple years and locations would help to validate and refine the models and tools developed here. The economic feasibility and long-term impacts of adopting this precision agriculture system also need to be assessed carefully, considering the specific costs, benefits, and risks for different types of farmers and farming systems in the region.

The other important recommendation is to use growing degree days (GDD) instead of the number of days since seeding to establish the relationship between LCC and GNDVI. Since temperature data is incorporated to calculate GDD, the model can be used regardless of the area in which it was developed. However, the data acquisition process will be complicated for the end-users as they have to measure temperature and include it in the application.

Another area of future research is the prototype software that has been built to showcase the model proposed in this study. A survey could be performed among the farmers to get information on what the end users need in the software. Since the software built for this study is just a prototype and not a final product, new features could be added. For instance, users could have the ability to store and run a time series analysis of soybean growth, which will help to make management decisions.

Future research could also focus on exploring machine learning and artificial intelligence techniques, which could also help improve the accuracy and automation of data analysis and decision support. Finally, engaging directly with farmers and other stakeholders through participatory research and extension efforts will ensure the relevance, usability, and adoption of precision agriculture innovations in Northwestern Ontario.

In conclusion, this thesis makes a significant contribution to precision agriculture by demonstrating the potential of low-cost remote sensing and web-based decision support tools for improving soybean production in the challenging growing conditions of Northwestern Ontario. While further research and development are needed to fully realize this potential, the findings and innovations presented here offer a promising foundation for advancing sustainable, resilient, and profitable farming systems in the region.

References

- Aeromotus. (2024) *Parrot SEQUOIA+ Multispectral Sensor*. Retrieved May 6, 2024, from <https://www.aeromotus.com/product/parrot-sequoia-multispectral-sensor/>.
- Ahmad, S., Kalra, A., & Stephen, H. (2010). Estimating soil moisture using remote sensing data: A machine learning approach. *Advances in Water Resources*, 33(1), 69–80. <https://doi.org/10.1016/J.ADVWATRES.2009.10.008>
- Ahmed, S. I., Rudra, R., Dickinson, T., & Ahmed, M. (2014). Trend and Periodicity of Temperature Time Series in Ontario. *American Journal of Climate Change*, 03(03), 272–288. <https://doi.org/10.4236/AJCC.2014.33026>
- Ahmed, S. I., Rudra, R., Goel, P., Amili, A., Dickinson, T., Singh, K., & Khan, A. (2022). Change in Winter Precipitation Regime across Ontario, Canada. *Hydrology*, 9(5), 81. <https://doi.org/10.3390/HYDROLOGY9050081/S1>
- Aklilu Tesfaye, A., & Gessesse Awoke, B. (2021). Evaluation of the saturation property of vegetation indices derived from sentinel-2 in mixed crop-forest ecosystem. *Spatial Information Research*, 29(1), 109–121. <https://doi.org/10.1007/S41324-020-00339-5/FIGURES/11>
- Apogee Instruments. (2024). *MC-100 Chlorophyll Concentration Meter*. <https://www.apogeeinstruments.com/mc-100-chlorophyll-concentration-meter/>
- Auravant. (2021) *Vegetation indices and their interpretation: NDVI, GNDVI, MSAVI2, NDRE, and NDWI - Auravant*. Retrieved June 13, 2023, from <https://www.auravant.com/en/articles/precision-agriculture/vegetation-indices-and-their-interpretation-ndvi-gndvi-msavi2-ndre-and-ndwi/>
- Barrows, C., & Bulanon, D. M. (2017). Development of a low-cost multispectral camera for aerial crop monitoring. *Journal of Unmanned Vehicle Systems*, 5(4), 192–200. <https://doi.org/10.1139/JUVS-2017-0008/ASSET/IMAGES/LARGE/JUVS-2017-0008F6.JPEG>
- Bogue, R. (2017). Sensors key to advances in precision agriculture. *Sensor Review*, 37(1), 1–6. <https://doi.org/10.1108/SR-10-2016-0215>
- Borotkanych, N. (2022). *Spatial Resolution In Remote Sensing: Which One To Choose?* <https://eos.com/blog/spatial-resolution/>
- Chapagain, T. (2017). Farming in Northern Ontario: Untapped Potential for the Future. *Agronomy 2017*, Vol. 7, Page 59, 7(3), 59. <https://doi.org/10.3390/AGRONOMY7030059>
- Climate LLC. (2023). *Climate FieldView*. <https://www.climatefieldview.ca/about/>
- CropX Inc. (2024). *CropX Agronomic Farm Management System*. <https://cropx.com/about-us/>
- da Silva, E. E., Rojo Baio, F. H., Ribeiro Teodoro, L. P., da Silva Junior, C. A., Borges, R. S., & Teodoro, P. E. (2020). UAV-multispectral and vegetation indices in soybean grain yield prediction based on in situ observation. *Remote Sensing Applications: Society and Environment*, 18, 100318. <https://doi.org/https://doi.org/10.1016/j.rsase.2020.100318>

- de Borja Reis, A. F., Moro Rosso, L., Purcell, L. C., Naeve, S., Casteel, S. N., Kovács, P., Archontoulis, S., Davidson, D., & Ciampitti, I. A. (2021). Environmental Factors Associated With Nitrogen Fixation Prediction in Soybean. *Frontiers in Plant Science*, *12*.
<https://doi.org/10.3389/FPLS.2021.675410/PDF>
- Django Software Foundation. *The web framework for perfectionists with deadlines | Django*. Retrieved May 7, 2024, from <https://www.djangoproject.com/>
- Durante, M., Oesterheld, M., Piñeiro, G., & Vassallo, M. M. (2014). Estimating forage quantity and quality under different stress and senescent biomass conditions via spectral reflectance. *International Journal of Remote Sensing*, *35*(9), 2963–2981.
<https://doi.org/10.1080/01431161.2014.894658>
- EOS Data Analytics Inc. (2024). *EOSDA Crop Monitoring: Farm Software For Agricultural Sector*.
<https://eos.com/products/crop-monitoring/>
- ESRI. (2023). *2D, 3D & 4D GIS Mapping Software | ArcGIS Pro*. <https://www.esri.com/en-us/arcgis/products/arcgis-pro/overview>
- Eugenio, F. C., Grohs, M., Venancio, L. P., Schuh, M., Bottega, E. L., Ruoso, R., Schons, C., Mallmann, C. L., Badin, T. L., & Fernandes, P. (2020). Estimation of soybean yield from machine learning techniques and multispectral RPAS imagery. *Remote Sensing Applications: Society and Environment*, *20*, 100397. <https://doi.org/10.1016/J.RSASE.2020.100397>
- Evans, J. R., & Clarke, V. C. (2019). The nitrogen cost of photosynthesis. *Journal of Experimental Botany*, *70*(1), 7–15. <https://doi.org/10.1093/JXB/ERY366>
- Fathi, M., & Shah-Hosseini, R. (2023). AUTOMATIC CORN AND SOYBEAN MAPPING BASED ON DEEP LEARNING METHODS (CASE STUDY: HAMILTON, HARDIN, BOONE, STORY, DALLAS, POLK, AND JUSPER COUNTIES IN IOWA STATE). *ISPRS Annals of the Photogrammetry, Remote Sensing and Spatial Information Sciences*, *X-4-W1-2022*(4/W1-2022), 187–193. <https://doi.org/10.5194/ISPRS-ANNALS-X-4-W1-2022-187-2023>
- Fensham, R. J., & Fairfax, R. J. (2002). Aerial photography for assessing vegetation change: a review of applications and the relevance of findings for Australian vegetation history. *Australian Journal of Botany*, *50*(4), 415–429. <https://doi.org/10.1071/BT01032>
- Finnan, J. M., Burke, J. I., & Jones, M. B. (1997). A Note on a Non-Destructive Method of Chlorophyll Determination in Wheat (*Triticum aestivum* L.). *Irish Journal of Agricultural and Food Research*, *36*(1), 85–89. <http://www.jstor.org/stable/25562295>
- Fujiwara, R., Kikawada, T., Sato, H., & Akiyama, Y. (2022). Comparison of Remote Sensing Methods for Plant Heights in Agricultural Fields Using Unmanned Aerial Vehicle-Based Structure From Motion. *Frontiers in Plant Science*, *13*. <https://doi.org/10.3389/fpls.2022.886804>
- Funk, L. (2020). *Providing Sustainable Protein for Global Nutrition Needs, Part 1 of 2 - U.S. Soy*.
<https://ussoy.org/providing-sustainable-protein-for-global-nutrition-needs-part-1-of-2/>
- Gaitán, J. J., Bran, D., Oliva, G., Ciari, G., Nakamatsu, V., Salomone, J., Ferrante, D., Buono, G., Massara, V., Humano, G., Celdrán, D., Opazo, W., & Maestre, F. T. (2013). Evaluating the performance of multiple remote sensing indices to predict the spatial variability of ecosystem

- structure and functioning in Patagonian steppes. *Ecological Indicators*, 34, 181–191.
<https://doi.org/10.1016/J.ECOLIND.2013.05.007>
- Gayathri Devi, K., Sowmiya, N., Yasoda, K., Muthulakshmi, K., & Kishore, B. (2020). REVIEW ON APPLICATION OF DRONES FOR CROP HEALTH MONITORING AND SPRAYING PESTICIDES AND FERTILIZER. *Journal of Critical Reviews*, 7(6), 667–672.
<https://doi.org/10.31838/JCR.07.06.117>
- Gitelson, A. A., Kaufman, Y. J., & Merzlyak, M. N. (1996). Use of a green channel in remote sensing of global vegetation from EOS-MODIS. *Remote Sensing of Environment*, 58(3), 289–298.
[https://doi.org/10.1016/S0034-4257\(96\)00072-7](https://doi.org/10.1016/S0034-4257(96)00072-7)
- Hafeez, A., Husain, M. A., Singh, S. P., Chauhan, A., Khan, Mohd. T., Kumar, N., Chauhan, A., & Soni, S. K. (2023). Implementation of drone technology for farm monitoring & pesticide spraying: A review. *Information Processing in Agriculture*, 10(2), 192–203.
<https://doi.org/https://doi.org/10.1016/j.inpa.2022.02.002>
- Han, H., Liu, Z., Li, J., & Zeng, Z. (2024). Challenges in remote sensing based climate and crop monitoring: navigating the complexities using AI. *Journal of Cloud Computing 2024 13:1*, 13(1), 1–14. <https://doi.org/10.1186/S13677-023-00583-8>
- Haskett, J. D., Pachepsky, Y. A., & Acock, B. (2000). Effect of climate and atmospheric change on soybean water stress: a study of Iowa. *Ecological Modelling*, 135(2–3), 265–277.
[https://doi.org/10.1016/S0304-3800\(00\)00369-0](https://doi.org/10.1016/S0304-3800(00)00369-0)
- Huete, A. R. (1988). A soil-adjusted vegetation index (SAVI). *Remote Sensing of Environment*, 25(3), 295–309. [https://doi.org/10.1016/0034-4257\(88\)90106-X](https://doi.org/10.1016/0034-4257(88)90106-X)
- IBIS World. (2023). *Soybean Farming in Ontario - Market Size, Industry Analysis, Trends and Forecasts (2024-2029)* | IBISWorld. <https://www.ibisworld.com/ca/industry/ontario/soybean-farming/14457/>
- Johnson, L. A., & Myers, D. J. (1995). Industrial Uses for Soybeans. *Practical Handbook of Soybean Processing and Utilization*, 380–427. <https://doi.org/10.1016/B978-0-935315-63-9.50025-5>
- Karson, M. (1968). Handbook of Methods of Applied Statistics. Volume I: Techniques of Computation Descriptive Methods, and Statistical Inference. Volume II: Planning of Surveys and Experiments. I. M. Chakravarti, R. G. Laha, and J. Roy, New York, John Wiley; 1967, \$9.00. *Journal of the American Statistical Association*, 63(323), 1047–1049.
<https://doi.org/10.1080/01621459.1968.11009335>
- Kaur, J., Hazrati Fard, S. M., Amiri-Zarandi, M., & Dara, R. (2022). Protecting farmers' data privacy and confidentiality: Recommendations and considerations. *Frontiers in Sustainable Food Systems*, 6, 903230. <https://doi.org/10.3389/FSUFS.2022.903230/BIBTEX>
- Kganyago, M., Mhangara, P., & Adjorlolo, C. (2021). Estimating Crop Biophysical Parameters Using Machine Learning Algorithms and Sentinel-2 Imagery. *Remote Sensing 2021, Vol. 13, Page 4314*, 13(21), 4314. <https://doi.org/10.3390/RS13214314>
- Khan, A., Shabir, D., Ahmad, P., -, al, Shaojuan Li, C., Lu, J., Pope, E., Prawira-Atmaja, M. I., Khomaini, H. S., Maulana, H., Harianto, S., & Rohdiana, D. (2018). Changes in chlorophyll and polyphenols content in *Camellia sinensis* var. *sinensis* at different stage of leaf maturity. *IOP Conference Series: Earth and Environmental Science*, 131(1), 012010. <https://doi.org/10.1088/1755-1315/131/1/012010>

- Kornilov, A. S., & Safonov, I. V. (2018). An Overview of Watershed Algorithm Implementations in Open Source Libraries. *Journal of Imaging*, 4(10). <https://doi.org/10.3390/jimaging4100123>
- Kross, A., Fernandes, R., Seaquist, J., & Beaubien, E. (2011). The effect of the temporal resolution of NDVI data on season onset dates and trends across Canadian broadleaf forests. *Remote Sensing of Environment*, 115(6), 1564–1575. <https://doi.org/10.1016/J.RSE.2011.02.015>
- Lakehead University Agricultural Research Station. *Who We Are | Lakehead University*. Retrieved May 29, 2023, from <https://www.lakeheadu.ca/centre/luars/who>
- Lal, M., Singh, K. K., Srinivasan, G., Rathore, L. S., Naidu, D., & Tripathi, C. N. (1999). Growth and yield responses of soybean in Madhya Pradesh, India to climate variability and change. *Agricultural and Forest Meteorology*, 93(1), 53–70. [https://doi.org/10.1016/S0168-1923\(98\)00105-1](https://doi.org/10.1016/S0168-1923(98)00105-1)
- Li, M., Shamshiri, R. R., Schirrmann, M., & Weltzien, C. (2021). Impact of Camera Viewing Angle for Estimating Leaf Parameters of Wheat Plants from 3D Point Clouds. *Agriculture*, 11(6). <https://doi.org/10.3390/agriculture11060563>
- Liang, S., & Wang, J. (2020). Leaf area index. *Advanced Remote Sensing*, 405–445. <https://doi.org/10.1016/B978-0-12-815826-5.00010-6>
- Lillesand, T., Kiefer, R. W., & Chipman, J. (2015). *Remote Sensing and Image Interpretation, 7th Edition*. Wiley. <https://books.google.ca/books?id=eQXYBgAAQBAJ>
- Liu, H., Zhang, W., Wang, F., Sun, X., Wang, J., Wang, C., & Wang, X. (2023). Application of an improved watershed algorithm based on distance map reconstruction in bean image segmentation. *Heliyon*, 9(4), e15097. <https://doi.org/10.1016/J.HELIYON.2023.E15097>
- Mabrouk, Y., Hemissi, I., Salem, I. Ben, Mejri, S., Saidi, M., & Belhadj, O. (2018). Potential of Rhizobia in Improving Nitrogen Fixation and Yields of Legumes. *Symbiosis*. <https://doi.org/10.5772/INTECHOPEN.73495>
- Mahajan, G. R., Pandey, • R N, Sahoo, • R N, Gupta, • V K, Datta, • S C, Dinesh Kumar, •, Pandey, R. N., Sahoo, R. N., Gupta, V. K., Datta, S. C., & Kumar, D. (2017). Monitoring nitrogen, phosphorus and sulphur in hybrid rice (*Oryza sativa* L.) using hyperspectral remote sensing The results of the investigation. *Precision Agriculture*, 18, 736–761. <https://doi.org/10.1007/s11119-016-9485-2>
- Malvern Panalytical Inc. (2024). *ASD HandHeld 2: Hand-held VNIR - Spectroradiometer | Product support | Malvern Panalytical*. <https://www.malvernpanalytical.com/en/support/product-support/asd-range/fieldspec-range/handheld-2-hand-held-vnir-spectroradiometer>
- Mangewa, L. J., Ndakidemi, P. A., Alward, R. D., Kija, H. K., Bukombe, J. K., Nasolwa, E. R., & Munishi, L. K. (2022). Comparative Assessment of UAV and Sentinel-2 NDVI and GNDVI for Preliminary Diagnosis of Habitat Conditions in Burunge Wildlife Management Area, Tanzania. *Earth (Switzerland)*, 3(3), 769–787. <https://doi.org/10.3390/EARTH3030044/S1>
- Mapbox. (2018). *Rasterio: access to geospatial raster data — rasterio documentation*. <https://rasterio.readthedocs.io/en/stable/>
- Mapir Camera. (2021) *Survey3 Cameras*. Retrieved February 1, 2024, from <https://www.mapir.camera/collections/survey3>

- Mapir Camera. (2023). *Survey3N Camera - Red+Green+NIR (RGN, NDVI) - MAPIR CAMERA*. MAPIR CAMERA. <https://www.mapir.camera/products/survey3n-camera-red-green-nir-rgn-ndvi>
- Mapir Camera. (2024). *MAPIR Camera Control (MCC)*. <https://www.mapir.camera/products/mapir-camera-control>
- Mathspace. *Existence of an Inverse | Grade 11 Math | Ontario 11 Functions (MCR3U) | (2022)*. Retrieved March 17, 2024, from <https://mathspace.co/textbooks/syllabuses/Syllabus-460/topics/Topic-8682/subtopics/Subtopic-115113/>
- Ministry of Agriculture, Food and Rural Affairs. (2012). *Soybean Production in Ontario*. Retrieved February 25, 2024, from <https://omafra.gov.on.ca/english/crops/field/soybeans.html>
- Measure. (2021) *Micasense RedEdge-MX*. Retrieved May 6, 2024, from <https://drones.measur.ca/products/micasense-rededge-mx>
- Morgan, J. L., Gergel, S. E., & Coops, N. C. (2010). Aerial Photography: A Rapidly Evolving Tool for Ecological Management. *BioScience*, 60(1), 47–59. <https://doi.org/10.1525/BIO.2010.60.1.9>
- Mylona, P., Pawlowski, K., & Bisseling, T. (1995). Symbiotic Nitrogen Fixation. *The Plant Cell*, 7(7), 869. <https://doi.org/10.1105/TPC.7.7.869>
- Natural Resources Canada. (2015, November 20). *Spatial Resolution, Pixel Size, and Scale*. <https://natural-resources.canada.ca/maps-tools-and-publications/satellite-imagery-and-air-photos/tutorial-fundamentals-remote-sensing/satellites-and-sensors/spatial-resolution-pixel-size-and-scale/9407>
- Neild, R., & Seeley, M. (1977). Growing Degree Days Predictions for Corn and Sorghum Development and Some Applications to Crop Production in Nebraska. *Historical Research Bulletins of the Nebraska Agricultural Experiment Station*. <https://digitalcommons.unl.edu/ardhistrb/41>
- Nijland, W., de Jong, R., de Jong, S. M., Wulder, M. A., Bater, C. W., & Coops, N. C. (2014). Monitoring plant condition and phenology using infrared sensitive consumer grade digital cameras. *Agricultural and Forest Meteorology*, 184, 98–106. <https://doi.org/https://doi.org/10.1016/j.agrformet.2013.09.007>
- NV5 Geospatial Solutions Inc. (2024). *Geospatial Image Analysis Software | ENVI*. <https://www.nv5geospatialsoftware.com/Products/ENVI>
- Omia, E., Bae, H., Park, E., Kim, M. S., Baek, I., Kabenge, I., & Cho, B. K. (2023). Remote Sensing in Field Crop Monitoring: A Comprehensive Review of Sensor Systems, Data Analyses and Recent Advances. *Remote Sensing 2023, Vol. 15, Page 354, 15(2)*, 354. <https://doi.org/10.3390/RS15020354>
- Pagano, M. C., & Miransari, M. (2016). The importance of soybean production worldwide. *Abiotic and Biotic Stresses in Soybean Production: Soybean Production: Volume 1, 5*, 1–26. <https://doi.org/10.1016/B978-0-12-801536-0.00001-3>
- Pasimeni, M. R., Valente, D., Semeraro, T., Petrosillo, I., & Zurlini, G. (2018). Anthropogenic landscapes. *Encyclopedia of Ecology*, 472–481. <https://doi.org/10.1016/B978-0-12-409548-9.10602-5>

- Pearce, R. (2024). *Soybean production heading north* | *Farmtario*. <https://farmtario.com/guides/soybean-guide-2023/soybean-production-heading-north/>
- Peng, Y., Zhu, T., Li, Y., Dai, C., Fang, S., Gong, Y., Wu, X., Zhu, R., & Liu, K. (2019). Remote prediction of yield based on LAI estimation in oilseed rape under different planting methods and nitrogen fertilizer applications. In *Agricultural and forest meteorology: Vol. v. 271*. Elsevier B.V.
- Pereira, J. A., Vélez, S., Martínez-Peña, R., & Castrillo, D. (2023). Beyond Vegetation: A Review Unveiling Additional Insights into Agriculture and Forestry through the Application of Vegetation Indices. *J 2023, Vol. 6, Pages 421-436*, 6(3), 421–436. <https://doi.org/10.3390/J6030028>
- Phadikar, S., & Goswami, J. (2016). Vegetation indices based segmentation for automatic classification of brown spot and blast diseases of rice. *2016 3rd International Conference on Recent Advances in Information Technology (RAIT)*, 284–289. <https://doi.org/10.1109/RAIT.2016.7507917>
- Prabhakara, K., Dean Hively, W., & McCarty, G. W. (2015). Evaluating the relationship between biomass, percent groundcover and remote sensing indices across six winter cover crop fields in Maryland, United States. *International Journal of Applied Earth Observation and Geoinformation*, 39, 88–102. <https://doi.org/10.1016/J.JAG.2015.03.002>
- Purcell, L. C., Salmeron, M., & Ashlock, L. (2014). Soybean growth and development. *Arkansas Soybean Production Handbook, 197*, 1–8.
- Python 3.12.3 Documentation. Retrieved May 6, 2024, from <https://docs.python.org/3/>
- Raeva, P. L., Šedina, J., & Dlesk, A. (2018). Monitoring of crop fields using multispectral and thermal imagery from UAV. <https://doi.org/10.1080/22797254.2018.1527661>, 52(sup1), 192–201. <https://doi.org/10.1080/22797254.2018.1527661>
- Ramos-Giraldo, P., Reberg-Horton, C., Locke, A. M., Mirsky, S., & Lobaton, E. (2020). Drought Stress Detection Using Low-Cost Computer Vision Systems and Machine Learning Techniques. *IT Professional*, 22(3), 27–29. <https://doi.org/10.1109/MITP.2020.2986103>
- Ramos-Giraldo, P., Reberg-Horton, S. C., Mirsky, S., Lobaton, E., Locke, A. M., Henriquez, E., Zuniga, A., & Minin, A. (2020). Low-cost Smart Camera System for Water Stress Detection in Crops. *2020 IEEE SENSORS*, 1–4. <https://doi.org/10.1109/SENSORS47125.2020.9278744>
- Rimpika, Anushi, Manasa, S., N., A. K., Sharma, S., Thakur, A., Shilpa, & Sood, A. (2023). An Overview of Precision Farming. *International Journal of Environment and Climate Change*, 13(12), 441–456. <https://doi.org/10.9734/IJECC/2023/V13I123701>
- Roerdink, J., & Meijster, A. (2000). The Watershed Transform: Definitions, Algorithms and Parallelization Strategies. *FUNDINF: Fundamenta Informatica*, 41.
- Sahota, T. S., Vanderwees, W., Tulonen, P., Mitchell, A., & Boersch, M. (2013). *Northwestern Ontario Specialty Crop Market Report*.
- Sajid, S. S., & Hu, G. (2022). Optimizing Crop Planting Schedule Considering Planting Window and Storage Capacity. *Frontiers in Plant Science*, 13, 762446. <https://doi.org/10.3389/FPLS.2022.762446/BIBTEX>
- Samreen, T., Tahir, S., Arshad, S., Kanwal, S., Anjum, F., Nazir, M. Z., & Sidra-Tul-Muntaha. (2023). Remote Sensing for Precise Nutrient Management in Agriculture. *Environmental Sciences*

- Proceedings 2022, Vol. 23, Page 32, 23(1), 32.*
<https://doi.org/10.3390/ENVIRONSCIPROC2022023032>
- scikit-learn, (2007). Machine learning in Python — *scikit-learn 1.4.2 documentation*. Retrieved May 6, 2024, from <https://scikit-learn.org/stable/>
- Šesták, Z. (1963). CHANGES IN THE CHLOROPHYLL CONTENT AS RELATED TO PHOTOSYNTHETIC ACTIVITY AND AGE OF LEAVES. *Photochemistry and Photobiology*, 2(2), 101–110. <https://doi.org/10.1111/J.1751-1097.1963.TB08207.X>
- Shafi, U., Mumtaz, R., García-Nieto, J., Hassan, S. A., Zaidi, S. A. R., & Iqbal, N. (2019). Precision Agriculture Techniques and Practices: From Considerations to Applications. *Sensors (Basel, Switzerland)*, 19(17). <https://doi.org/10.3390/S19173796>
- Shahi, T. B., Xu, C. Y., Neupane, A., & Guo, W. (2023). Recent Advances in Crop Disease Detection Using UAV and Deep Learning Techniques. *Remote Sensing 2023, Vol. 15, Page 2450, 15(9), 2450*. <https://doi.org/10.3390/RS15092450>
- Singh, V., & Misra, A. K. (2017). Detection of plant leaf diseases using image segmentation and soft computing techniques. *Information Processing in Agriculture*, 4(1), 41–49. <https://doi.org/10.1016/J.INPA.2016.10.005>
- Sishodia, R. P., Ray, R. L., & Singh, S. K. (2020). Applications of Remote Sensing in Precision Agriculture: A Review. *Remote Sensing 2020, Vol. 12, Page 3136, 12(19), 3136*. <https://doi.org/10.3390/RS12193136>
- Sony Electronics Inc. (2019). *What is the relationship between aperture, shutter speed, and ISO? | Sony USA*. <https://www.sony.com/electronics/support/articles/00025973>
- Sozzi, M., Marinello, F., Pezzuolo, A., & Sartori, L. (2018). Benchmark of satellites image services for precision agricultural use. *Proceedings of the AgEng Conference, Wageningen, The Netherlands*, 8–11.
- Stamford, J. D., Violet-Chabrand, S., Cameron, I., & Lawson, T. (2023). Development of an accurate low cost NDVI imaging system for assessing plant health. *Plant Methods*, 19(1), 1–19. <https://doi.org/10.1186/S13007-023-00981-8/FIGURES/10>
- Stein, H. H., Berger, L. L., Drackley, J. K., Fahey, G. C., Hernot, D. C., & Parsons, C. M. (2008). Nutritional Properties and Feeding Values of Soybeans and Their Coproducts. *Soybeans: Chemistry, Production, Processing, and Utilization*, 613–660. <https://doi.org/10.1016/B978-1-893997-64-6.50021-4>
- Survey3: Multispectral Survey Cameras - MAPIR CAMERA. Retrieved June 17, 2023, from <https://www.mapir.camera/pages/survey3-cameras>
- Suwanpravit, C., & Srichai, N. (2012). Impacts of spatial resolution on land cover classification. *Proceedings of the Asia-Pacific Advanced Network*, 33(0), 39. <https://doi.org/10.7125/APAN.33.4>
- Toth, C., & Józków, G. (2016). Remote sensing platforms and sensors: A survey. *ISPRS Journal of Photogrammetry and Remote Sensing*, 115, 22–36. <https://doi.org/10.1016/j.isprsjprs.2015.10.004>
- Tucker, C. J. (1979). Red and photographic infrared linear combinations for monitoring vegetation. *Remote Sensing of Environment*, 8(2), 127–150. [https://doi.org/10.1016/0034-4257\(79\)90013-0](https://doi.org/10.1016/0034-4257(79)90013-0)

- Ustin, S. L., & Jacquemoud, S. (2020). How the optical properties of leaves modify the absorption and scattering of energy and enhance leaf functionality. *Remote Sensing of Plant Biodiversity*, 349–384. https://doi.org/10.1007/978-3-030-33157-3_14/FIGURES/16
- Vásquez, R. A. R., Heenkenda, M. K., Nelson, R., & Segura Serrano, L. (2023). Developing a New Vegetation Index Using Cyan, Orange, and Near Infrared Bands to Analyze Soybean Growth Dynamics. *Remote Sensing*, 15(11). <https://doi.org/10.3390/rs15112888>
- VertMarkets, Inc. (2022). *FieldSpec HandHeld*. Retrieved February 10, 2024, from <https://www.laboratorynetwork.com/doc/fieldspec-handheld-0001>
- Wang, C., Feng, M. C., Yang, W. De, Ding, G. W., Sun, H., Liang, Z. Y., Xie, Y. K., & Qiao, X. X. (2016). Impact of spectral saturation on leaf area index and aboveground biomass estimation of winter wheat. *Spectroscopy Letters*, 49(4), 241–248. <https://doi.org/10.1080/00387010.2015.1133652>
- Weather Spark. *Climate and Average Weather Year Round in Thunder Bay*. Retrieved May 19, 2023, from <https://weatherspark.com/y/12875/Average-Weather-in-Thunder-Bay-Canada-Year-Round#Figures-Temperature>
- Xue, J., & Su, B. (2017). Significant remote sensing vegetation indices: A review of developments and applications. *Journal of Sensors*, 2017. <https://doi.org/10.1155/2017/1353691>
- Yue, J., Feng, H., Jin, X., Yuan, H., Li, Z., Zhou, C., Yang, G., & Tian, Q. (2018). A Comparison of Crop Parameters Estimation Using Images from UAV-Mounted Snapshot Hyperspectral Sensor and High-Definition Digital Camera. *Remote Sensing*, 10(7). <https://doi.org/10.3390/rs10071138>
- Zanin, A. R. A., Neves, D. C., Teodoro, L. P. R., da Silva Júnior, C. A., da Silva, S. P., Teodoro, P. E., & Baio, F. H. R. (2022). Reduction of pesticide application via real-time precision spraying. *Scientific Reports 2022 12:1*, 12(1), 1–12. <https://doi.org/10.1038/s41598-022-09607-w>
- Zhang, J., Wang, C., Yang, C., Xie, T., Jiang, Z., Hu, T., Luo, Z., Zhou, G., & Xie, J. (2020). Assessing the effect of real spatial resolution of in situ UAV multispectral images on seedling rapeseed growth monitoring. *Remote Sensing*, 12(7), 1207.
- Zhang, Y., Li, Y., Wang, R., Xu, L., Li, M., Liu, Z., Wu, Z., Zhang, J., Yu, G., & He, N. (2020). Spatial Variation of Leaf Chlorophyll in Northern Hemisphere Grasslands. *Frontiers in Plant Science*, 11. <https://doi.org/10.3389/FPLS.2020.01244/PDF>
- Zhang, Z., & Zhu, L. (2023). A Review on Unmanned Aerial Vehicle Remote Sensing: Platforms, Sensors, Data Processing Methods, and Applications. *Drones*, 7(6). <https://doi.org/10.3390/drones7060398>